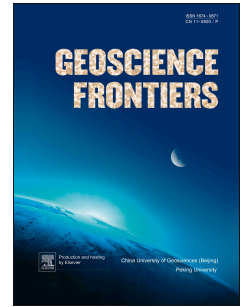


Accepted Manuscript

Interaction between protokimberlite melts and mantle lithosphere: evidence from mantle xenoliths from the Dalnyaya kimberlite pipe, Yakutia (Russia)

I.V. Ashchepkov, T. Ntaflos, Z.V. Spetsius, R.F. Salikhov, H. Downes



PII: S1674-9871(16)30051-2

DOI: [10.1016/j.gsf.2016.05.008](https://doi.org/10.1016/j.gsf.2016.05.008)

Reference: GSF 458

To appear in: *Geoscience Frontiers*

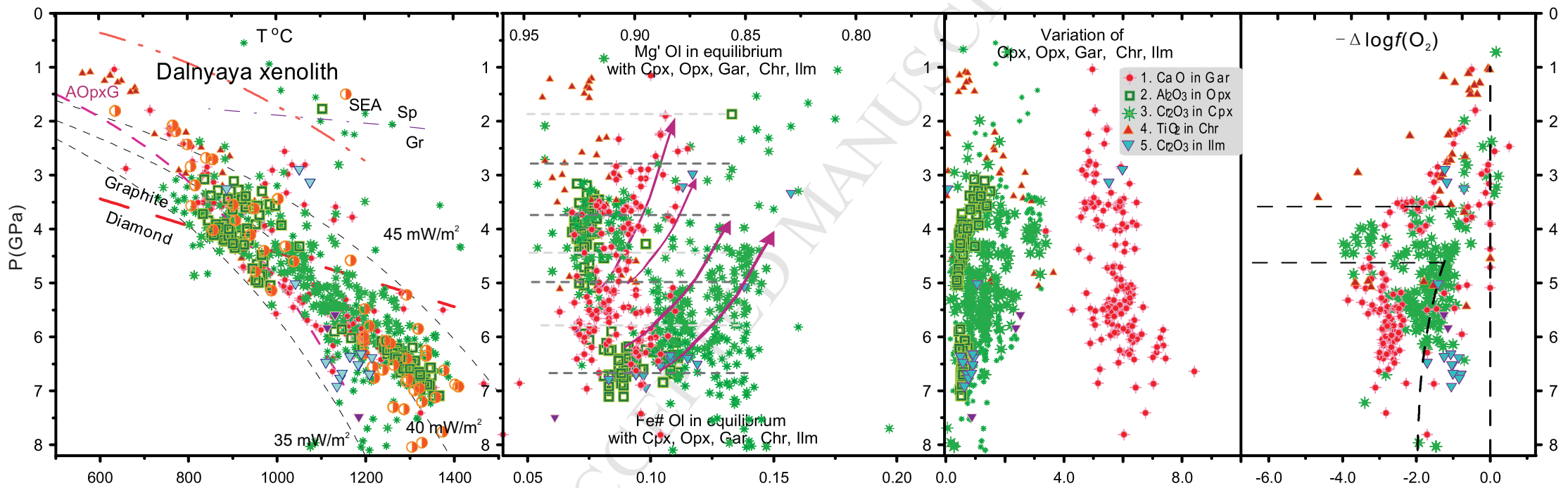
Received Date: 26 January 2016

Revised Date: 27 April 2016

Accepted Date: 1 May 2016

Please cite this article as: Ashchepkov, I.V., Ntaflos, T., Spetsius, Z.V., Salikhov, R.F., Downes, H., Interaction between protokimberlite melts and mantle lithosphere: evidence from mantle xenoliths from the Dalnyaya kimberlite pipe, Yakutia (Russia), *Geoscience Frontiers* (2016), doi: 10.1016/j.gsf.2016.05.008.

This is a PDF file of an unedited manuscript that has been accepted for publication. As a service to our customers we are providing this early version of the manuscript. The manuscript will undergo copyediting, typesetting, and review of the resulting proof before it is published in its final form. Please note that during the production process errors may be discovered which could affect the content, and all legal disclaimers that apply to the journal pertain.



1 **Interaction between protokimberlite melts and mantle lithosphere: evidence from mantle**
2 **xenoliths from the Dalnyaya kimberlite pipe, Yakutia (Russia)**

3 I.V. Ashchepkov^{a,*}, T. Ntaflos^b, Z.V. Spetsius^c, R.F. Salikhov^c, H. Downes^d

4 ^a *Institute of Geology and Mineralogy, SD RAS, Koptyug avenue 3, 63090, Novosibirsk, Russia*

5 ^b *Vienna University, A-1090 Vienna, Austria*

6 ^c *Alrosa Stock Company, Mirny, Lenina 6, Russia*

7 ^d *Department of Earth and Planetary Sciences, Birkbeck University of London, London, UK*

8

9 *Corresponding author e-mail address: Igor.Ashchepkov@igm.nsc.ru; garnet@igm.nsc.ru;
10 igora57@mail.ru

11 phone (fax): 007-950-5918327

12 fax institute: 007 -383-2332792

13

14

15

16

17 **Abstract**

18 The Dalnyaya kimberlite pipe (Yakutia, Russia) contains mantle peridotite xenoliths
19 (mostly lherzolites and harzburgites) that show both sheared porphyroclastic (deformed) and
20 coarse granular textures, together with ilmenite and clinopyroxene megacrysts. Deformed
21 peridotites contain high-temperature Fe-rich clinopyroxenes, sometimes associated with
22 picroilmenites, which are products of interaction of the lithospheric mantle with protokimberlite
23 related melts. The orthopyroxene-derived geotherm for the lithospheric mantle beneath
24 Dalnyaya is stepped similar to that beneath the Udachnaya pipe. Coarse granular xenoliths fall
25 on a geotherm of 35 mWm^{-2} whereas deformed varieties yield a 45 mWm^{-2} geotherm in the 2–
26 7.5 GPa pressure interval. The chemistry of the constituent minerals including garnet, olivine
27 and clinopyroxene shows trends of increasing $\text{Fe}^\#$ ($= \text{Fe}/(\text{Fe}+\text{Mg})$) with decreasing pressure. This
28 may suggest that the interaction with fractionating protokimberlite melts occurred at different
29 levels. Two major mantle lithologies are distinguished by the trace element patterns of their
30 constituent minerals, determined by LA-ICP-MS. Orthopyroxenes, some clinopyroxenes and
31 rare garnets are depleted in Ba, Sr, HFSE and MREE and represent relic lithospheric mantle. Re-
32 fertilized garnet and clinopyroxene are more enriched. The distribution of trace elements
33 between garnet and clinopyroxene shows that the garnets dissolved primary orthopyroxene and
34 clinopyroxene. Later high temperature clinopyroxenes related to the protokimberlite melts
35 partially dissolved these garnets. Olivines show decreases in Ni and increases in Al, Ca and Ti
36 from Mg-rich varieties to the more Fe-rich, deformed and refertilized ones. Minerals showing
37 higher $\text{Fe}^\#$ (0.11–0.15) are found within intergrowths of low-Cr ilmenite-clinopyroxene-garnet
38 related to the crystallization of protokimberlite melts in feeder channels. In P - $f(\text{O}_2)$ diagrams,
39 garnets and Cr-rich clinopyroxenes indicate reduced conditions at the base of the lithosphere at -
40 5 log units below a FMQ buffer. However, Cr-poor clinopyroxenes, together with ilmenite and
41 some Fe-Ca-rich garnets, demonstrate a more oxidized trend in the lower part of lithosphere at -2
42 to 0 log units relative to FMQ. Clinopyroxenes from xenoliths in most cases show conditions
43 transitional between those determined for garnets and megacrystalline Cr-poor suite. The
44 relatively low diamond grade of Dalnyaya kimberlites is explained by a high degree of
45 interaction with the oxidized protokimberlite melts, which is greater at the base of the
46 lithosphere.

47 Key words: mantle xenoliths; trace element; melt interaction; kimberlite; pyrope; Cr-
48 diopside

49

50

51 **1. Introduction**

52 Mantle xenoliths brought to the surface by kimberlite eruptions show a wide variety of
53 compositions and textures. One of the most important problems in understanding the formation
54 such xenoliths is determining primary features (i.e. those present in the mantle before kimberlite
55 activity began) and secondary ones superimposed on the mantle peridotites prior to (or during)
56 entrainment in the host kimberlite. Here we present a study of mantle material from the
57 Dalnyaya kimberlite pipe in Siberia giving evidence for interaction of the mantle with
58 fractionating protokimberlite melts.

59 The Dalnyaya pipe, discovered in 1955, is one the largest kimberlite pipes (390×270 m)
60 in the Daldyn field. Like most large pipes in the central part of the Yakutian kimberlite province
61 (YKP) (Fig. 1A), Dalnyaya has a Late Devonian age (Agashev et al., 2004; Zaitsev and Smelov,
62 2010; Smelov et al., 2014). It is located in the southeastern part of the Daldyn field (Fig. 1B).
63 The pipe is composed of two major group I (Mitchell, 1995) kimberlite varieties, both containing
64 large amounts of debris mainly macrocrystic olivine (Cas et al., 2008). Autolithic kimberlite
65 breccia (AKB) dominates the northern and eastern parts, whereas massive magmatic porphyritic
66 kimberlite (PK) forms bodies in the northern and southeastern parts. It has a relatively low
67 diamond grade compared to Aykhal, Udachnaya, Yubileinaya and other pipes which are being
68 mined, and its greater distance from the mining centers did not allow industrial exploration to
69 start earlier. Nevertheless, the overall diamond capacity is 10.2 million carats with total price of
70 about 600,000 dollars, has allowing industrial work to start (Interfax, 2015). In 2011 a new 30
71 m-deep prospecting quarry was excavated within the central part of the pipe which is composed
72 of PK, in contact with AKB. Both kimberlite varieties contain large amounts of mantle xenoliths,
73 dominantly peridotites with relatively fresh pyroxenes and olivines.

74 In this paper, we have investigated mineral compositions from xenoliths and concentrates
75 of both PK and ABK facies using electron probe micro analyzes (EPMA) and LA-ICP-MS, and
76 have reconstructed the mantle section beneath the pipe as has been previously done for the
77 Sytykanskaya pipe (Ashchepkov et al., 2015). The occurrence of abundant Cr-poor, Fe-rich
78 clinopyroxenes and the unusually large amounts of ilmenite intergrowths and ilmenite-bearing
79 xenoliths, including garnet wehrlites and Cr-bearing peridotites, suggest a high degree of
80 interaction of protokimberlites with mantle peridotites, which probably influenced the diamond
81 grade.

82

83 **2. Samples**

84 All ~300 xenoliths studied were collected from the newly excavated quarry in August-
85 September, 2012. They are relatively fresh and contain fresh pyroxenes and even olivines.
86 Commonly they are 3-10 cm in size. We did not separate samples from AKB and PK in this
87 study. The latter contains more abundant and fresher xenoliths, but megacrysts and their
88 intergrowth in AKB are more abundant. Large garnet-ilmenite-clinopyroxene intergrowths
89 described in previous publications (Rodionov et al., 1988, 1991) were not found, because the
90 quarry mainly exposes PK facies.

91

92 **3. Analytical methods**

93 Preliminary analyses were made of 40 xenoliths in thin-section using the Camebax Micro
94 electron microprobe in IGM SB RAS. In addition, more than 75 xenoliths were analyzed in thin
95 sections at the University of Vienna. For more than 30 high precision microprobe analyses were
96 done for two crystals per sample. We also analyzed minerals from concentrates of PK (370) and
97 ABK (420) facies separately, whereas minerals of an additional ~50 mantle xenoliths were
98 analyzed in grain-mounts. Previous studies of the Dalnyaya pipe were devoted to the comparison
99 of indicator minerals between the two kimberlite phases (Rodionov et al., 1984), and to the
100 intergrowths of pyrope garnet, clinopyroxene and ilmenite megacrysts, and the ilmenite-bearing
101 peridotites and pyroxenites (Rodionov et al., 1988, 1991). Analyses from a previous study of
102 ilmenite-chromite-diopside intergrowths (Ashchepkov et al., 2014) were also included in the data
103 base as well as analyses of ilmenite-bearing garnet pyroxenites from Rodionov et al. (1988,
104 1991) and Genshaft et al. (1987).

105 The procedure of the Electron Probe Microanalysis (EPMA) used for the analyses of
106 concentrates and xenoliths in mounts in IGM SB RAS is described by Lavrent'ev et al. (1987).
107 Routine conditions and precision of the analyses of Camebax Micro microprobe were also
108 published (Sobolev et al., 1973, 2009a; Lavrent'ev and Usova, 1994; Ashchepkov et al., 2010a,
109 2012, 2013a,b, 2014, 2015). The detailed work on xenoliths (75) in thin sections was done at the
110 University of Vienna using a Cameca100-SX microprobe. All analyses were done using mineral
111 standards with wavelength-dispersive spectrometers; acceleration voltage and beam current were
112 15 kV and 20 nA, respectively, and standard correction procedures were applied. Trace elements
113 in olivines from xenoliths were also performed with the Cameca 100SX. For the high precision

114 analyses of olivine, the acceleration voltage of 20 kV, a slightly defocused beam current of 60
115 nA were applied. In order to increase the precision and reduce the effect of noisy background on
116 very low elemental concentrations, a 120 second counting time on peak position and on both low
117 and high background positions, were used. As standard for the major elements (Si, Fe, Mg, Ca)
118 natural olivine was used and for Ni, Cr, Al, Mn, metal alloys was used. Precision varies from 7
119 to 25 ppm for trace elements in olivine like Ni, Cr, Al, Mn and Ca.

120 Mineral concentrates were analyzed by laser ablation inductively coupled LA-
121 ICP-MS at the Analytic Centre of IGM SB RAS (Ashchepkov et al., 2008). An additional 52
122 LA-ICP-MS analyses were obtained with the same equipment for minerals in thin sections of the
123 xenoliths studied by EPMA in Vienna University (Supplementary File 1, Tables 1, 2). Analyses
124 of trace elements of xenoliths in mounts and thin sections were obtained by LA- ICP-MS
125 methods using a Finnegan Element I mass spectrometer and laser ablation system Nd YAG: UV
126 New Wave 133 nm in Analytic Center of IGM SD RAS. The details were described in previous
127 publications (Ashchepkov et al., 2012, 2013a, b, c, 2014a, b, 2015; Afanasiev et al., 2014).

128

129

130 **4. Petrographic description of the xenoliths**

131 The set of >300 xenoliths covers the petrographic variations in the lithospheric mantle
132 beneath the Dalnyaya pipe (Fig. 2). Most of them are rather small (1 to 3 cm) and it is difficult to
133 judge their structure using such small amounts of material.

134 The xenoliths belong to both the green Cr-bearing suite and black low-Cr suite described
135 in previous publications (Rodionov et al., 1993). Most of them are relatively fertile or depleted
136 garnet lherzolites (Fig. 2I) (25 vol. %) and harzburgites (Fig. 2P, U) (15 vol. %) (Fig. 3). Garnets
137 in fertile xenoliths are only partly altered but in coarse grained harzburgites they are intensely
138 kelyphitized. Many xenoliths (> 45 vol. %) contain bright emerald-green Cr-diopsides which
139 form veins and micro-veins (Fig. 2E, Q, W), sometimes together with rather large bright red
140 rounded garnets. Xenoliths which are unusually enriched in garnets and clinopyroxenes (Fig. 2G,
141 J), (i.e. tending towards garnet websterites) constitute 5–7 vol. % of the studied collection.
142 Garnet dunites (Fig. 2X) are very scarce (1–2 vol. %). Spinel harzburgites (Fig. 2p) comprise
143 >12–10 vol. %. Giant-grained pyroxenites with parallel lamellae of orthopyroxene and rare
144 garnets (Fig. 2D) occur very rarely (<2 vol. %). Typical eclogites were not discovered in this

145 collection but clinopyroxene-garnet-ilmenite intergrowths were described previously (Rodionov
146 et al., 1988, 1991).

147 Garnet peridotites frequently show porphyroclastic textures (Fig. 2H, K, L, R) with two
148 generations of olivine and intergranular Cr-diopsides. Sometimes olivine aggregates are grouped
149 into clusters which may originally represent large olivine grains are now recrystallized (Fig. 2H,
150 K, R). The coarse-grained peridotites are rare and mainly are represented by depleted
151 harzburgites with or without garnet. Some xenoliths are composed of rounded polycrystalline
152 fragments (Fig. 2T) cut by dark aggregates including pyroxenes, ilmenites (Fig. 2M) and
153 sulfides cemented by more Fe-rich olivines. Ilmenite grains commonly together with Fe-rich
154 pyroxenes are located in intergranular spaces together with mica and sulfides which are often
155 replaced by djerfisherite. Ilmenite peridotites from Dalnyaya are texturally unequilibrated (Fig.
156 2M, Q) and differ from those found in Sytykanskaya (Ashchepkov et al., 2015) and Udachnaya
157 pipes (Pokhilenko et al., 1976). Abundant mica veinlets were found in one Dalnyaya peridotite,
158 and in rare cases mica is accompanied by richterite amphiboles (Supplementary File 4).

159 In the Dalnyaya megacryst associations, ilmenite is more abundant than garnet and
160 chromite. Elliptical ilmenite nodules up to 8 cm in diameter often containing clinopyroxene and
161 olivine inclusions and intergrowths (Fig. 2A, B, C) occur in the ABK. Garnet-ilmenite-
162 clinopyroxene associations including giant-grained varieties are more common in ABK facies
163 than in PK.

164

165 **5. Chemistry of minerals**

166 Compositions of pyrope garnets from concentrates mostly fall in the lower part of the lherzolite
167 field (Sobolev et al., 1973) with concentrations of Cr_2O_3 reaching 13 wt. %. Some plot in the
168 harzburgite and even dunite fields (Fig. 3), whereas garnets from xenoliths generally fall in the
169 lherzolite field. Wehrlitic garnet megacrysts or those from the low-Ca xenolith suite contain up
170 to 2.5 wt. % Cr_2O_3 or even belong to the Cr-rich group. The Cr-rich garnets from xenoliths have
171 higher TiO_2 concentrations. The PK contain higher amount of both sub-calcic and pyroxenitic
172 garnets compared to xenoliths and ABK garnet populations.

173 All Cr-bearing clinopyroxenes from the kimberlite heavy fractions have low Al contents.
174 A few Al-rich varieties (up to 6 wt. % Al_2O_3) are found among the Fe-rich samples (up to 4.5 wt.
175 % FeO) in ilmenite-bearing and porphyroclastic peridotites (Fig. 4). Na_2O contents, together
176 with Cr_2O_3 and MgO, decrease with increasing FeO, whereas TiO_2 is nearly constant.

177 Orthopyroxenes which contain 4–5 wt. % FeO show increases of Al₂O₃ and CaO
178 (Supplementary File 2, Fig. 3), decreases of Cr₂O₃ and NiO, and high scatter in TiO₂. As the
179 content of FeO reaches 7 wt. %, Al₂O₃ and Cr₂O₃ decrease and CaO and TiO₂ become constant.

180 Ilmenites from AKB and PK show similar trends but the latter shows higher scatter in
181 NiO, Al₂O₃ and Cr₂O₃. Two sub-trends dividing at 51 wt. % TiO₂ are seen in ilmenites from the
182 AKB (Fig. 5). The first show stable Cr₂O₃ contents at ~ 0.9 wt. % whereas Mg- and Ti-rich
183 varieties show variations in Cr₂O₃ ~0.5–1.2 wt. % and dispersion of other components.

184 Ilmenites in the peridotite xenoliths, as well as those from the intergrowths with
185 clinopyroxenes, belong mainly to the Mg-rich type (up to 16 wt. % MgO). Significant
186 differences in the TiO₂–Al₂O₃ trends suggest that ilmenites from AKB and PK were formed in
187 different stages. However, ilmenites from Dalnyaya do not show the division into three groups
188 which is typical for the pipes from the Zarnitsa cluster (Amshinsky and Pokhilenko, 1983).

189 Chromites are rarely found in the xenoliths; they occur mostly in the rims of garnets and
190 in the Garnet-free chromite-bearing lherzolites. They show three major intervals in Cr₂O₃ and
191 only a few plot within the diamond window. In chromite from the xenoliths, TiO₂ enrichment
192 increases with Cr₂O₃ (i.e. with increasing pressure) (Fig. 6), but Cr-content is much higher (35–
193 55 wt. % Cr₂O₃) in chromites from the concentrates.

194 Phlogopites are relatively scarce in xenoliths from Dalnyaya compared with the Alakit
195 field pipes like Sytykanskaya (Ashchepkov et al., 2015). Most phlogopites occupy positions in
196 the variation diagrams just on the boundary between scattered grains and typical micro-veined
197 phlogopite-bearing associations and may relate to interaction with intergranular melts as was
198 determined for xenoliths from the Sytykanskaya pipe (Ashchepkov et al., 2015) (Fig. 7).

199 The richterite amphiboles from Dalnyaya xenoliths are K-Na type (see Supplementary
200 File 4) and differ from those found in peridotite xenoliths from Alakit kimberlites which are
201 mostly K-rich (Ashchepkov et al., 2015).

202 Four large clusters and six small groups of olivines can be distinguished from their
203 variations of trace components vs. Fe[#]. The first cluster (I) is a low-Fe group (Fe[#] = 0.05–0.6)
204 which comprises relic peridotites corresponding to Archean dunites. Cluster II with Fe[#]=0.07–
205 0.9 is composed of fertile peridotites, whereas several samples (Cluster III) with Fe[#]=0.09–0.10
206 may be related to refertilized peridotites. We consider that the most Fe-rich group (Cluster IV)
207 with Fe[#]=0.11–0.13 is related to interaction with protokimberlite melts. In general, the magmatic
208 components Ca, Al, Mn show increases with Fe[#], but Ti and Cr demonstrate more complex

209 trends in separate intervals (Fig. 8). General decrease of Ni is common and is explained by
210 interaction with the essentially carbonatitic and kimberlite melts (Bussweiler et al., 2014).

211

212 **6. Thermobarometry**

213 ***6.1 Comparison of pressure-temperature (PT) estimates for mantle lithosphere beneath*** 214 ***the Dalnyaya pipe***

215 The pyroxene geotherm with the inflection at 6 GPa (Boyd, 1973) constructed for
216 Lesotho was reproduced for sub-continental lithospheric mantle (SCLM) beneath Udachnaya in
217 Daldyn field (Boyd et al., 1997) and appeared again for the SCLM beneath Dalnyaya pipe.

218 *P–T* estimates based on orthopyroxene thermobarometry yield the most reliable geotherm
219 according to our comparisons (Ashchepkov et al., 2010, 2011, 2012, 2013a, b, c, 2014). Opx
220 barometry was widely used in mantle reconstructions (Finnerty and Boyd, 1984). We used for
221 the construction of the simple and reliable geotherm the combination (McGregor, 1974; Brey
222 and Kohler, 1990) (Fig. 9A). Opx-based and Gar-Opx methods (Nickel and Green, 1985; Nickel,
223 1989; Brey and Kohler, 1990) (Fig. 9A, B, C) respectively, with the Opx or Opx-Cpx (Brey and
224 Kohler, 1990) thermometers produce nearly coinciding PT plots (Wu and Zhao, 2011).

225 The mantle lithosphere beneath the Dalnyaya pipe is layered and shows two major
226 pressure intervals with a gap from 5 to 6 GPa, while beneath the Udachnaya pipe this interval is
227 represented by coarse Gar-harzburgites and eclogites (Ashchepkov et al., 2012, 2014) (see
228 Supplementary File 2, Fig. 5). In the SCLM beneath Udachnaya there are 6 definite layers in the
229 lithospheric mantle and the number of rock-types is higher (Ashchepkov et al., 2010, 2013b;
230 2014; Ionov et al., 2010). At least four groups from the lower and middle part of the Dalnyaya
231 mantle section are close or nearly the same as those determined from the Udachnaya SCLM (see
232 Supplementary File 2, Fig. 5B). The low-T group from 5 to 6 GPa is represented on *P–T* diagram
233 for Dalnyaya by several points. The middle group corresponding to a pyroxenite layer
234 (Pokhilenko et al., 1999) is cooler. The shallowest groups which are common in Udachnaya
235 SCLM are not represented, mainly because the samples with large Cpx and Gar grains were
236 analyzed while the shallow depleted harzburgites were omitted.

237 Comparison of different combinations of thermometers and barometers shows that PT
238 estimates using Gar-Opx barometry (Nickel and Green, 1985; Brey and Kohler, 1990) (Fig.
239 9A,B,C) practically reproduces the Opx geotherm. The Cr–Cpx -based geotherm (Nimis and

240 Taylor, 2000) (Fig. 9D) reproduces the same groups as the Opx-based PT points but show
 241 displacement to higher pressures for the Fe-Cr-bearing compositions. The Cpx method based on
 242 jadeite-diopside exchange for the peridotitic and pyroxenitic associations (Ashchepkov et al.,
 243 2011) (Fig. 9E) shows that the high pressure branch composed of the sheared and
 244 porphyroclastic peridotites consists of two separate groups which differ in temperature. In
 245 general, it produces the much higher temperature geotherm probably related to the
 246 protokimberlite stage. This universal Cpx-based thermobarometry which could be applied to the
 247 low-Cr basic and Cr-rich ultrabasic and eclogitic systems (Ashchepkov et al., 2011) (Fig. 9 E)
 248 also traces all the Opx-points but the proportion of the high temperature associations is much
 249 greater. The reason is not only in the difference in thermometry but also that the lower-Cr
 250 associations were not used for thermometry by Cr-Cpx methods.

251 The garnet geotherm (Ashchepkov et al., 2015) (Fig.9E) traces practically all the groups
 252 of the orthopyroxene geotherm but continues into the higher pressure part, showing that the
 253 interval from 6 to 5 GPa is rather depleted in orthopyroxenes as well as the low pressure part.

254 The chromite-based geotherm (Supplementary File 2, Fig.5) corresponds mainly to the
 255 middle and low pressure intervals. Ilmenite-based PT estimates from the xenoliths
 256 (Supplementary File 2, Fig.5) reflect the conditions of high pressure interactions in the lower
 257 part of the mantle section and of mantle metasomatism in the middle part accompanied by
 258 formation of phlogopite and amphiboles.

259

260 ***6.2 P - T - X - $f(O_2)$ reconstructions of mantle sections***

261 The P - T - $f(O_2)$ estimates based on the monomineral thermobarometry (Ashchepkov et al.,
 262 2010, 2012, 2013a, b, c, 2014a, b, 2015) enable us to make PTXfO₂ diagrams for all xenoliths
 263 samples together (Fig. 10A) and separately for the concentrates (Fig. 10B, C) as was previously
 264 done for the Sytykanskaya pipe (Ashchepkov et al., 2015). In general, the geotherm for minerals
 265 from xenoliths is very similar to that for the mantle beneath the Udachnaya pipe (Ashchepkov et
 266 al., 2013). The P -Fe[#] plot shows several garnet trends demonstrating increasing Fe[#] with
 267 decreasing pressure (see the arrows) which are common in mantle columns worldwide (Fig. 10A,
 268 B, C) (Ashchepkov et al., 2010, 2012, 2013a, b, c). Clinopyroxene and even olivine (pressure
 269 determined from the associated Cpx) repeats these trends; possibly this is the result of some
 270 rapidly differentiated melts in different pressures in the mantle column formed in several stages.
 271 Clinopyroxene and ilmenites in P -Fe[#] plot often relate to the most Fe-rich branches

272 corresponding to the Ilm-Cpx intergrowths near the lithosphere base. The P - T - X - $f(\text{O}_2)$ diagram
 273 for the xenoliths shows that many associations are not equilibrated, the Cpx are often much more
 274 Fe-rich compared to the garnets and olivines and this is not a temperature- dependent Fe-Mg
 275 distribution (Krogh, 1988; Kohler and Brey, 1990). The garnet P -CaO trends are divided into
 276 three lines with different CaO contents. The higher values are typical for garnets near the
 277 lithosphere asthenosphere boundary (LAB) and the highest values are in garnets of the
 278 pyroxenite-wehrlite associations. They are related to fertilization processes produced by
 279 carbonatitic protokimberlite melts (Howarth et al., 2014; Pokhilenko et al., 2015).

280 The P - T - X diagrams based on minerals from the concentrates are divided (Fig. 10B,C)
 281 into two parts at 4.0 GPa. The P - $\text{Fe}^\#$ trends show a rapid increase of FeO with decreasing
 282 pressures corresponding to the evolution of ilmenite trend produced by the protokimberlites. The
 283 AKB concentrates demonstrate some enrichment of garnets in CaO and FeO from 3.5 to 4.5 GPa
 284 compared with those from PK. This suggests the presence of pyroxenites in the middle part of
 285 the mantle column. The ilmenite trend in P - $\text{Fe}^\#$ diagrams is divided into two intervals at
 286 $\text{Fe}^\#=0.12$, probably related to two stages of protokimberlite evolution.

287 In the P - $f(\text{O}_2)$ diagram (Fig. 10), the garnets and several clinopyroxenes near 5 GPa show
 288 a trend which is common for the SCLM worldwide (McCammon et al., 2001; McCammon and
 289 Kopylova, 2004), showing increasingly reduced conditions with depth. The ilmenite trend traces
 290 the diamond stability as in the Sytykanskaya pipe (Ashchepkov et al., 2015) which suggests
 291 relatively close $f(\text{O}_2)$ conditions for megacrystic associations derived from protokimberlites and
 292 megacrystic clinopyroxenes. Some increase in $f(\text{O}_2)$ occurs in the lower part of the SCLM and
 293 several garnet points are located within the oxidized field, coinciding with the oxygen fugacity
 294 conditions for the ilmenites and clinopyroxenes, which in general resemble the oxygen fugacity
 295 of protokimberlite melts (Höfer et al., 2009).

296 This highly oxidized level is marked also by several Gar, Cpx and Ilm points near 3 GPa.
 297 Oxidized associations correspond to the essentially carbonatitic compositions of the kimberlitic
 298 parental melts, according to the lines of CO_3^{2-} concentrations (Stagno et al., 2013).

299 The P - T - X - $f(\text{O}_2)$ diagrams for the xenoliths (Fig. 10A) also show the presence of two
 300 major pressure intervals in SCLM divided at 3.5 GPa. The lower part shows a high degree of
 301 heating which is commonly associated with sheared mantle and is often related to interaction
 302 with protokimberlite melts (Agashev et al., 2013; Ashchepkov et al., 2013b) as in the SCLM
 303 beneath the Udachnaya pipe. However, in the Dalnyaya pipe they are represented by
 304 porphyroclastic and micro-veined peridotites. Their P - T points on diagram (Figs. 9, 10) are

305 marked by orthopyroxene, orthopyroxene-garnet and clinopyroxene thermobarometry and form
 306 convection branch below 6 GPa (Boyd et al., 1997). Clinopyroxene P - T estimates yield hotter
 307 geotherms compared with those produced by other minerals. Temperatures based on the two
 308 pyroxene methods (Wells, 1977; Taylor et al., 1979; Brey and Kohler, 1990) are higher than
 309 those that are orthopyroxene-based (Brey and Kohler, 1990). So the orthopyroxene-based
 310 geotherms are essentially cooler than Cpx-only estimates (Nimis and Taylor, 2000). The
 311 common Gar-Opx barometry (Nickel and Green, 1985; Brey and Kohler, 1990) in combination
 312 with the two pyroxene temperature gives similar or slightly hotter conditions than the
 313 orthopyroxene-based method.

314 Garnets in the P - $Fe^{\#}$ diagram reveal linear trends in the lower part of diagram and also in
 315 the upper part which definitely differ from those determined for concentrates from kimberlites.
 316 The upper interval is divided at 3.0–2.5 GPa showing irregular heating and increasing of $Fe^{\#}$ for
 317 garnets and pyroxenes. The lowest pressure interval 1.0–2.0 GPa is again highly heated and
 318 represented by the Fe-rich associations.

319 The P - $f(O_2)$ diagram for garnets from xenoliths shows a linear decreasing $f(O_2)$ trend
 320 from -3.5 to -1.5 ΔFMQ in the pressure interval from 7.5 to 2GPa, which is narrower than the
 321 range shown by the minerals from concentrates (Fig. 10A). Ilmenites from the xenoliths show a
 322 rather wide range in Cr_2O_3 up to 6 wt. % at near 3.5 GPa. Clinopyroxenes mostly correspond to
 323 more oxidizing conditions than garnets. The presence of several Ilm P - $Fe^{\#}$ trends as well as for
 324 Gar and Cpx suggest that the lower and middle parts of the peridotite mantle column were
 325 subject to several stages of melt percolation.

326

327 **7. Trace elements**

328 **7.1. Trace elements in peridotitic minerals**

329 Trace element concentrations in garnet, clinopyroxene and ilmenite grains from the
 330 concentrates (Supplementary File 1, Tables 1, 2) and xenoliths are generally very similar (Figs.
 331 11, 12). Garnets mainly show HREE-enriched round patterns, although those from concentrates
 332 have higher HREE compared with those from xenoliths, which show a dominant harzburgitic
 333 pattern with a slight depression from Yb to Dy or sometimes a humped pyroxenitic pattern with
 334 a peak at Sm (Fig. 11C). All garnets have strong depressions in Sr, Ba, Zr-Hf and Ta-Nb.
 335 Garnet of dunitic type has deep trough from Sm to Yb. Garnets from the mineral concentrates
 336 from kimberlites mostly have similar round patterns. Some of them show slightly lower HREE

337 content and only one belongs to the depleted dunitic type with the inflected REE pattern close to
338 S-type, but it does not show a deep high field strength element (HFSE) trough (Supplementary
339 File 2, Fig. 13).

340 Among the clinopyroxenes, the dominant type shows an asymmetric bell-like pattern
341 with a peak at Nd and nearly flat patterns from Ta to Rb with troughs at Ba, Hf and deeper
342 troughs at Zr and Pb. (Fig. 11A). The other clinopyroxenes show various patterns; two have REE
343 patterns with an inflection in Eu and Gd and are similar in incompatible trace elements to garnets
344 with deep Ba and Pb troughs. Two others show inflected or sinusoidal REE patterns with
345 inflections in Gd and Dy and elevated incompatible elements with peaks in Nb and Pb (Fig.
346 11D).

347 All olivines have W-shaped REE patterns with abundances range from 1 to 0.01 relative
348 to primitive mantle (PM) (McDonough and Sun, 1995) with local elevation near Gd and Tb.
349 Most olivines show depressions in Ba, Sr, Y, Zr, Hf, Nb, Ta and a peak at Pb. Orthopyroxene
350 shows a more enriched U-shaped REE near 0.1/PM and trace element spider diagram similar to
351 those from mantle xenoliths from Bezymianny (Ionov et al., 2013) with peaks in Th, U, Hf and
352 troughs or elevated Ta, Nb, Y. The only analyzed phlogopite (intergrowing with olivine) reveals
353 peaks in Ba, Sr, Pb, elevated HFSE especially Zr but a trough in Y (Fig. 11D).

354

355 *7.2 Trace elements in minerals from low-Cr suite*

356 Ilmenite intergrowths with clinopyroxenes represent the low-Cr suite (Moore and
357 Belousova, 2005). Clinopyroxenes from the intergrowths in general are similar to those of
358 magmatic-type clinopyroxenes from lherzolites but some peaks in U and Ba. Trace element
359 patterns in the ilmenites in intergrowths in general are nearly the same as those from megacrysts
360 (Fig. 12A). They mostly have low abundances and W-shaped REE patterns with inflections in
361 Gd and Eu, as in orthopyroxenes. In trace element spider diagrams they show peaks in Nb–Ta
362 and Zr–Hf with smaller peaks in Pb but minima in Y. Two other enriched ilmenite grains
363 demonstrate concave, inclined patterns in REE and elevated incompatible elements group but
364 nearly the same levels in HFSE and without Y anomalies.

365 The trace element patterns for the minerals from the concentrates are in general very
366 similar to those analyzed in xenoliths. But most of the clinopyroxenes belong to the low-Cr
367 varieties and are closer to the high temperature Cpx from xenoliths and Ilm intergrowth and
368 show patterns which are close to those from the associations described above (Fig. 12B).

369

370 **8. Discussion**371 **8.1. Comparison of *P–T–X* sections of Dalnyaya with other mantle columns beneath**372 ***YKP***

373 The mantle column beneath the Dalnyaya pipe shows some special features compared to
374 those beneath other pipes in the Daldyn field. Garnet trends in the P – $Fe^{\#}$ diagram consist of
375 several branches of increasing $Fe^{\#}$. Starting from the LAB at least four different levels occur in
376 the mantle column, which may represent the traces of rising and differentiating melts. The
377 deepest level (7–5.5 GPa) corresponds to the minimum effective viscosity of the mantle in the
378 presence of melts (Karato, 2010) or water (Peslier, 2010) or an increase in oxygen fugacity,
379 features which are commonly combined as a result of intrusion of protokimberlite melts
380 (Goncharov et al., 2012; Doucet et al., 2014). Local shearing in the upper levels is also possible
381 in the presence of melts and volatiles (Katayama et al., 2009). Possibly this took place in the
382 mantle beneath Dalnyaya because deformed varieties yield rather high pressure ranges from >7
383 to 4.5 GPa.

384 Compared to the mantle sections beneath other large pipes in the Daldyn field such as
385 Udachnaya and Zarnitsa, the Dalnyaya mantle section does not show the presence of eclogites
386 and, even in the concentrates, orange eclogite-type garnets are not frequent.

387 The double P – CaO trend detected for garnets in Dalnyaya xenoliths, is most likely a sign
388 of the reactions with Ca-rich melts, because Ca-riched varieties are typical for the high
389 temperature varieties show signs of re-fertilization. The presence of sub-calcic garnets, which
390 form several clots and trends in the lower part of the mantle section, suggests a rather high
391 diamond grade of this pipe. The P – CaO trend for analyzed xenoliths with large amount of garnet
392 and clinopyroxene is nearly constant within the 3–6 GPa interval, probably as a result of the
393 influence of evolving melts. Evolving intergranular melts probably also had some influence.
394 Pyroxenites showing most variability in compositions and TRE content are found mainly near
395 the LAB and within the middle pyroxenite layer.

396

397 **8.2 Trace elements evidence for mantle peridotite evolution**

398 From trace element geochemistry, two major types of peridotites exist in the lithospheric
399 mantle beneath Dalnyaya. The first group is characterized by negative anomalies in Ba, Sr, Pb

400 and sometimes Y and Nb–Ta. These features are found mainly in orthopyroxenes, some garnets
401 and two clinopyroxenes. The other lithology corresponds to mantle that has interacted with
402 plume-related melts, possibly protokimberlites. They are enriched in Ba, Sr and HFSE and have
403 lower LILE concentrations. We tried to determine the tendencies of the changes of major and
404 trace elements of different minerals in different levels of the mantle column.

405 Olivines show several trends of enrichments in Ti, Al, Ca vs Pressure (GPa), on the
406 (Supplementary File 2, Fig.9A), which probably relates to the evolution of the melts with which
407 they were in equilibrium. Greater enrichment of magma-related components occurs near the
408 LAB.

409 Clinopyroxenes also show enrichment of Sr^* ($Sr^* = \sqrt{Nd_n \times Sm_n}$), Pb, U/Pb, Zr and Y with
410 slightly decreasing pressure. This may mean that reaction with the intruded melts occurred in 3
411 separate intervals probably corresponding to intermediate magma chambers for the
412 protokimberlite melts. In the top of each interval corresponding to 6, 4.5 and 2.5 GPa, where
413 melt concentration should be higher, the degree of interaction with wall-rock peridotites is also
414 more intense. Increasing Ni in clinopyroxene shows the influence of ultramafic material or could
415 also possibly be a result of contamination as happened with Cr in ilmenites (Fig. 10A of
416 Supplementary File 2)

417 Garnets appear to have experienced major refertilization because their REE patterns are
418 not harzburgitic. Only four of them show sinusoidal REE patterns and may be related to the
419 primary type. There are correlations between the REE slope $((La/Yb)_N$ or $(Gd/Yb)_N$ and values of
420 Sr^* minima or Y^* , Pb^* , which results from the decrease of the slope for the parental melts
421 (Supplementary File 2, Fig. 10B) or degree of differentiation. The inclination of the HREE
422 garnet slopes in the mantle column decreases with increasing temperature which is explained by
423 mineral physics (Blundy and Wood, 1994). The degree of depletion is generally higher in the
424 upper part of the mantle. But some characteristics of relatively depleted harzburgite associations
425 are found for some garnets in the lower parts of the mantle.

426 The strong enrichment in the LILE components which commonly accompanies
427 phlogopite and amphibole metasomatism (Gregoire et al., 2002) was not detected for most
428 samples; only a few minerals in association with phlogopites show enrichment in Rb and Ba.
429 However, most garnets show Nb–Ta enrichment similar to those from the Arkhangelsk
430 kimberlite province (Afanasiev et al., 2013).

431

432 **8.3. Reconstructed parental melts for minerals from xenoliths**

433 The trace element compositions of melts reconstructed using K_D values (Hart and Dunn,
434 1993) for the main type of clinopyroxene related to refertilization almost completely coincide
435 with those of the kimberlite melts from Dalnyaya pipe, having a gentle inclined pattern with Sr
436 minimum (Kargin et al., 2011) and even a small Ta–Nb hump. Some clinopyroxenes reveal
437 primary lherzolitic features in their more complex spider-diagrams and higher $(La/Yb)_N$ ratios.
438 Formation of clinopyroxene in the sheared peridotites was caused by intrusion of protokimberlite
439 melts, which produced megacrysts, porphyroclastic and sheared peridotites (Ionov et al., 2010;
440 Agashev et al., 2013). Some peridotites with ovoid brecciated structures and veins with ilmenites
441 and associated clinopyroxenes are possibly the first step in the formation of polymict breccias
442 (Giuliani et al., 2013) (Fig. 13A).

443 The melts reconstructed from the garnets have different patterns depending on the
444 partition coefficient used (Hauri, 1994; Harte and Kirkley, 1997; Green et al., 2000; Bedard,
445 2006; Tuff and Gibson, 2007; Fulmer et al., 2010; Girnir et al., 2013; Katzyura et al., 2015) (see
446 Fig.8 of Supplementary File 2). If we use K_D for silicate melts (Green et al., 2000) which are
447 lower in HFSE and LILE compared to those for carbonatite-silicate melts (Girnir et al., 2013;
448 Katzyura et al., 2015), the obtained spider-diagrams show gently sloping patterns close to those
449 obtained for the clinopyroxenes, except for the HFSE which are closer to those of kimberlites
450 (Kargin et al., 2011). (Fig. 13C) Nevertheless the LREE for the clinopyroxene and garnet do not
451 coincide entirely, nor do Ta–Nb and Zr–Hf; furthermore garnet shows much lower $(La/Sm)_N$
452 ratios than clinopyroxene, demonstrating incomplete equilibration. Resulting in trace element
453 patterns almost completely coincide with clinopyroxene trace element spider-diagrams from
454 Vitim mantle melts (Ashchepkov et al., 2011) which are also typical for plume melts formed by
455 1 % melting of garnet peridotites. $(La/Sm)_N$ deviations in garnet and clinopyroxene suggests that
456 the melts which produced the garnets resulted from dissolution of primary clinopyroxenes. This
457 “garnetization” may be caused by addition of water expanding the stability field of garnets and
458 increasing pressure during ancient subduction.

459 The calculated melts for the olivines and orthopyroxene using partition coefficients after
460 Imai et al. (2012) and Bedard (2006) show REE patterns which are inflected in Gd and are
461 higher in LREE compared with melts in equilibrium with clinopyroxene (although this may
462 result from uncertainty in partition coefficient; Fig. 13B). These inflected patterns are a common
463 feature for most orthopyroxene from mantle xenoliths of Kamchatka (Ionov et al., 2013) and
464 other xenolith localities in subduction settings (Ishimaru and Arai, 2009) and probably reflect a

465 primary subducted nature for the peridotites. These melts mostly have negative anomalies of
466 Nd–Sm and Ta–Nb which are typical for subduction-related melts. However, U, Th and LILE
467 contents are similar to orthopyroxene from peridotite xenoliths from Bezymianny (Ionov et al.,
468 2013).

469 The reconstructed melts for the ilmenites estimated using K_D values of Zack and Brumm
470 (1998) with addition for HFSE (Klemme et al., 2006) in general have very similar REE patterns
471 to those determined for the megacrystic pyroxenites. But they are particularly high in HFSE and
472 Pb. The depression from La to Sm cannot be explained by chromatographic effects but is more
473 likely a result of selective removal of clinopyroxene from the rock, which may also explain the
474 W-shaped pattern for the parental melts of olivine and orthopyroxene. Only two ilmenites show
475 trace element multicomponent diagrams which resemble those of the host kimberlites (Kargin et
476 al., 2011).

477 We checked the equilibrium of the garnet-clinopyroxene pair using the partition
478 coefficients for clinopyroxene/garnet. In most cases they repeat the shapes of the K_D calculated
479 for the garnet lherzolites and harzburgites from the Finsch pipe (Gibson et al., 2008), which were
480 established to be equilibrated in trace elements and isotopic features (Lazarov et al., 2013). But
481 those from Dalnyaya with close K_D in REE show some disequilibrium features such as the
482 curved patterns in La–Nd and relative enrichment in the HFSE, which means that the parental
483 melts were much closer to kimberlitic than those parental to the garnets (Fig. 14A). However,
484 three K_D showing irregular patterns in REE diagrams related to clinopyroxene which was less
485 enrich trace components which did not react with protokimberlites as those analyzed in SCLM
486 beneath the Finsch pipe (Fig. 16 of Supplementary File 2).

487 Equilibrium between Cpx and Ilm in intergrowths is not complete. Only one sample
488 (D1175) shows a smooth partition coefficient pattern. We calculated the Ilm/melt partition. It
489 shows higher values of the HFSE than those determined by Zack and Brumm (1998) with similar
490 method for the Ilm-Cpx intergrowth from Hawaii cumulate basaltic xenoliths. However, the
491 calculated parental melts for ilmenites are even less enriched in REE than with the previous K_D
492 set (Fig. 14B).

493

494 ***8.4 Evolution of the melts in the mantle column beneath the Dalnyaya pipe***

495 We suggest that the relic associations of garnet-clinopyroxene and especially the
496 orthopyroxene with HFSE depressions may represent the ancient SCLM beneath the Daldyn

497 field. But they do not have positive anomalies at Pb, Sr and U which are the typical features of
498 subduction-related fluid and melts, so they represent rather deep material which did not
499 experience subduction.

500 Formation of the garnets with primitive round trace element patterns may be related to a
501 refertilization probably associated with plume melts. This event was definitely prior to intrusion
502 of the melts which created the shearing and metasomatism similar to processes in mantle column
503 beneath Udachnaya pipe (Solov'ev et al., 2012; Kostrovitsky et al., 2013; Agashev et al., 2013).
504 In general garnets and clinopyroxenes are essentially refertilized similar to the mantle beneath
505 Finsch pipe (Lazarov et al., 2012). It seems that ultramafic melt equilibrated with the peridotites
506 evidenced by the garnet and olivine from enriched refertilized peridotites having $Fe^{\#} = 0.09$ –
507 0.10. Some pyroxenes may have been equilibrated with these garnets but most of them are more
508 Fe-rich and closer to protokimberlites which, according to minerals from polymict breccias and
509 sheared peridotites, have $Fe^{\#} = 0.11$ –0.13. These large scale processes of interaction and
510 refertilization have also been found in many kimberlite localities such as Udachnaya (Howarth et
511 al., 2014; Pokhilenko et al., 2015) and are commonly associated with metasomatism by silicate-
512 carbonatite melts.

513 It seems that this was the stage close to the formation of the channels through which the
514 protokimberlite melt rose and in which megacrysts grew on the walls (Moore and Lock, 2002;
515 Ashchepkov et al., 2014). This was followed by an increase of temperature and interaction with
516 protokimberlite melts accompanied by an increase of Fe, Ca and Ti. The more Fe-rich varieties
517 may represent samples of the low-Cr suite, which may be related to contact zones with the
518 protokimberlite melt. Formation of ilmenites with depleted W-shaped REE patterns may be due
519 to interaction of melts with rather depleted peridotite because melts commonly move through
520 olivine-rich aggregates. Clinopyroxenes, olivine and one orthopyroxene found as inclusions in
521 the ilmenite nodules are not the result of exsolution or pegmatoid intergrowth (Haggerty et al.,
522 1975) but look like material captured by the kimberlite mush or later inflows of the
523 protokimberlite melts. Thus, we can suggest a multistage evolution of the mantle beneath
524 Dalnyaya pipe as was suggested for the Kaapvaal craton (Konzett et al., 2013).

525

526 ***8.5. Schemes of refertilization***

527 The PTX diagrams show that refertilizing melts were intruded at several levels in the
528 SCLM, at 6.5, 5.5 and 4.5 GPa according to clinopyroxene thermobarometry (Figs. 11 and 12).

529 The diagrams for the garnets show that they also occurred in the 3-2 GPa level. The changes of
530 characteristic ratios and incompatible elements from relatively fertile to more depleted in the
531 upper part of the mantle section suggest that refertilization originated in the asthenosphere. We
532 measured the garnets for trace elements mainly from the hot branch. The agents that caused
533 refertilization should be related to the last plume event. The question is why the garnets are not
534 equilibrated with the clinopyroxenes. It is likely that garnets were growing when the distant most
535 evolved melts with higher carbonatite fractions were interacting with the peridotites, dissolving
536 original orthopyroxenes and clinopyroxenes and thus they are richer in CaO than the garnets
537 from the low temperature branch (Fig. 12). In turn, clinopyroxenes with higher HREE than in
538 equilibrated peridotites from Finsch (Lazarov et al., 2013) should have dissolved some garnet
539 material. They grew later during increasing interaction near the developing channels and in many
540 cases show great compositional variations. A possible mechanism is that intruded melts were
541 rising the intergranular spaces, accompanied by differentiation (Burgess and Harte, 2004), i.e.,
542 assimilation fractionation crystallization (AFC) (De Paolo, 1984). This would be followed by an
543 increase of the incompatible elements together with the typical peridotitic components. The
544 second possibility is that the melts evolved in separate chambers and rose up step by step so that
545 the interaction took place mainly near the chambers and feeders.

546 The high temperature Fe-rich clinopyroxenes show an increase of Cr with decreasing
547 pressures. It is likely that that this is AFC with contamination of parental melts derived from
548 peridotites. But ilmenites which possibly crystallized from a separate liquid show a small
549 increase of Cr during ascent.

550 Modeling of AFC with different schemes (Fig. 15) including dissolution of garnets (or
551 clinopyroxene) and crystallization of clinopyroxenes (or garnet) or both together from partial
552 lherzolite melts (Ashchepkov et al., 2011) or kimberlite melts (Kargin et al., 2011) (Figs. 17–20
553 in Supplementary File 2) shows some similarities with the analyzed natural garnets and
554 clinopyroxenes (Fig. 14A, B, Fig. 15). Dissolution of clinopyroxene explains the bell-like REE
555 patterns for the garnets but cannot explain minima in HREE. Dissolution of garnet explains the
556 elevated HREE of clinopyroxene. Trace element components could be reduced by contamination
557 in orthopyroxenes and increase in HFSE content after ilmenite dissolution. It is possible to show
558 how the trace element components could be reduced by contamination in orthopyroxenes and
559 increasing HFSE content rises after ilmenite dissolution (Fig. 15D). Using uncontaminated
560 kimberlites compositions without HFSE anomalies (referring to melting degree $F \sim 1\%$) or partial
561 melts from primitive peridotites close to basalts ($F \sim 1\%$) (Ashchepkov et al., 2011) can satisfy
562 the flat incompatible elements part of the original trace element compositions of garnets if we

563 use a K_D for silicate melts (e.g. Green et al., 2000). But using carbonatite-silicate melt
564 coefficients (Girmis et al., 2013; Kazyura et al., 2015) produces elevated HFSE patterns.
565 However, many garnet compositions show flat HREE minima from Ho to Yb which could be
566 derived from the original depleted source. It is necessary to melt a major amount of
567 orthopyroxenes or another mineral to form U-shaped HREE pattern. Orthopyroxene melting is a
568 common model for silica enrichment of carbonatitic kimberlite melts (Brett et al., 2015).

569

570 ***8.6. Significance of melt interaction for diamond grade***

571 The relatively low diamond grade of the Dalnyaya pipe could be the result of several
572 processes. First is the high degree of mantle metasomatism by highly oxidized melts. This is
573 visible also in the NS mantle transect (Fig. 21 in Supplementary File 2) of the SCLM from the
574 Daldyn field. Nearly half of the clinopyroxenes from xenoliths fall outside the diamond stability
575 field in the P - fO_2 diagrams, together with the ilmenites. The very low concentration of eclogites
576 and pyroxenites is also an unfavorable factor because nearly half of the diamonds in productive
577 kimberlites belong to the eclogite type, according to their inclusions (Sobolev et al., 2004;
578 Logvinova et al., 2005). The amount of sub-calcic garnets, which probably were produced by
579 percolation of reduced fluid in Archean time (Klein-Ben David et al., 2014) within the dunite
580 channels (Pearson and Wittig, 2014), is also relatively low compared to the other large pipes.

581

582 ***9. Conclusions***

- 583 (1) The peridotite mantle beneath the Dalnyaya pipe underwent multistage metasomatism and,
584 was affected by oxidized melts related to protokimberlites during the final stage;
- 585 (2) Many mineral associations in the mantle column are not thermally and chemically
586 equilibrated;
- 587 (3). The lithospheric mantle beneath the Dalnyaya pipe is layered and consists of five stepped
588 layers which were heated to different degrees;
- 589 (4). The SCLM beneath Dalnyaya contains very small amounts of eclogites and pyroxenites and
590 originally was built up by peridotites which could be island arc-type, but lack the signs of U, Sr,
591 Ba subduction-related metasomatism.

592

593 **Acknowledgements**

594 We are very thankful to ALROSA Company for help in sampling. Many thanks to S.V.
595 Palessky for the performing of the LA-ICP-MS measurements and to O.S. Khmelnikova for help
596 in microprobe measurements on Camebax Micro in Analytic Centre IGM SB RAS. The works
597 are supported by RBRF grants: 05-05-64718, 11-05-00060; 11-05-91060-PICS; 16-05-00860.
598 The work contains the result of the projects 77-2, 65-03, 02-05 UIGGM SD RAS and ALROSA
599 Stock Company.

600

601 **References**

- 602 Afanasiev, V.P., Ashchepkov, I.V., Verzhak, V.V., O' Brien, H., Palessky, S.V., 2013.
603 PT conditions and trace element variations of picroilmenites and pyropes from the Arkhangelsk
604 region. *Journal of Asian Earth Sciences* 70, 45-63.
- 605 Agashev A.M., Pokhilenko N.P., Tolstov A.V., Polyanichko N.P., Mal'kovets V.G.,
606 Sobolev N.V., 2004. New data on age of kimberlites from Yakutian kimberlite province.
607 *Doklady Earth sciences RAN* 399, 95–99.
- 608 Agashev, A. M., Ionov, D. A., Pokhilenko, N. P., Golovin, A. V., Cherepanova, Yu,
609 Sharygin, I. S., 2013. Metasomatism in lithospheric mantle roots: Constraints from whole-rock
610 and mineral chemical composition of deformed peridotite xenoliths from kimberlite pipe
611 Udachnaya. *Lithos* 160, 201-215.
- 612 Amshinsky, A.N., Pokhilenko, N.P., 1983. Peculiarities of the picroilmenite
613 compositions from Zarnitsa kimberlite pipe (Yakutia). *Russian Geology and Geophysics* 24 (11),
614 116-119.
- 615 Arndt, N.T., Guitreau, M., Boullier, A.-M. leRoex, A., Tommasi, A., Cordier, P.,
616 Sobolev A., 2010. Olivine, and the origin of kimberlite. *Journl of Petrology* 51 (3), 573–602.
- 617 Ashchepkov, I.V., Pokhilenko, N.P., Vladykin, N.V., Logvinova, A.M., Kostrovitsky,
618 S.I., Afanasiev, V.P., Pokhilenko, L.N., , Kuligin, S.S., Malygina, L.V., Alyмова, N.V.,
619 Khmelnikova, O.S., Palessky, S.V., Nikolaeva, I.V., Karpenko, M.A., Stagnitsky, Y.B., 2010.
620 Structure and evolution of the lithospheric mantle beneath Siberian craton, thermobarometric
621 study. *Tectonophysics* 485, 17-41.
- 622 Ashchepkov, I.V., André, L., Downes, H., Belyatsky, B.A., 2011. Pyroxenites and
623 megacrysts from Vitim picrite-basalts (Russia): Polybaric fractionation of rising melts in the
624 mantle? *Journal of Asian Earth Sciences* 42, 14-37.
- 625 Ashchepkov, I.V., Rotman, A.Y., Somov, S.V., Afanasiev, V.P., Downes, H., Logvinova,

- 626 A.M., Nossyko, S. Shimupi, J., Palessky, S.V., Khmelnikova, O.S., Vladykin, N.V., 2012.
 627 Composition and thermal structure of the lithospheric mantle beneath kimberlite pipes from the
 628 Catoca cluster, Angola. *Tectonophysics* 530, 128-151
- 629 Ashchepkov, I.V., Vladykin, N.V., Ntaflos, T., Downes, H., Mitchel, R., Smelov, A.P.
 630 Rotman, A.Ya., Stegnitsky, Yu., Smarov, G.P., Makovchuk, I.V., Nigmatulina, E.N.,
 631 Khmelnikova, O.S., 2013a. Regularities of the mantle lithosphere structure and formation
 632 beneath Siberian craton in comparison with other cratons. *Gondwana Research* 23, 4-24.
- 633 Ashchepkov, I.V., Ntaflos, T., Kuligin, S.S., Malygina, E.V., Agashev, A.M., Logvinova,
 634 A.M., Mityukhin, S.I., Alymova, N.V., Vladykin, N.V., Palessky, S.V., Khmelnikova, O.S.,
 635 2013b. Deep-Seated Xenoliths from the Brown Breccia of the Udachnaya Pipe, Siberia. D. G.
 636 Pearson et al. (eds.). *Proceedings of 10th International Kimberlite Conference*. - New Delhi:
 637 Springer India, v. 1., 59-74.
- 638 Ashchepkov, I.V., Downes, H., Mitchell, R., Vladykin, N.V., Coopersmith, H., Palessky,
 639 S.V., 2013c. Wyoming Craton Mantle Lithosphere: Reconstructions Based on Xenocrysts from
 640 Sloan and Kelsey Lake Kimberlites. In: Pearson D. G. et al. (eds.) *Proceedings of 10th*
 641 *International Kimberlite Conference*. - New Delhi: Springer India, v. 1. 13-27
- 642 Ashchepkov I.V., Vladykin N.N., Ntaflos T., Kostrovitsky S.I., Prokopiev S.A., Downes
 643 H., Smelov A.P., Agashev A.M., Logvinova A.M., Kuligin S.S., Tychkov N.S., Salikhov R.F.,
 644 Stegnitsky Yu.B., Alymova N.V., Vavilov M.A., Minin V.A., Babushkina S.A.,
 645 Ovchinnikov Yu.I., Karpenko M.A., Tolstov A.V., Shmarov G.P., 2014a. Layering of the
 646 lithospheric mantle beneath the Siberian Craton: Modeling using thermobarometry of mantle
 647 xenolith and xenocrysts *Tectonophysics* 634, 55-75.
- 648 Ashchepkov I. V. , Alymova N. V., Logvinova A. M., Vladykin N. V., Kuligin S. S.,
 649 Mityukhin S. I., Downes H., Stegnitsky Yu. B., Prokopiev S.A., Salikhov R.F., Palessky V. S.,
 650 Khmel'nikova O. S., 2014b. Picroilmenites in Yakutian kimberlites: variations and genetic
 651 models. *Solid Earth* 5, 915-938.
- 652
- 653 Ashchepkov, I.V., Logvinova, A.M., Reimers, L.F., Ntaflos, T., Spetsius, Z.V., Vladykin,
 654 N.V., Downes, H., Yudin, D.S., Travin, A.V., Makovchuk, I.V. and Palesskiy, V.S., 2015. The
 655 Sytykanskaya kimberlite pipe: Evidence from deep-seated xenoliths and xenocrysts for the
 656 evolution of the mantle beneath Alakit, Yakutia, Russia. *Geoscience Frontiers* 6(5), 687-714.
- 657 Ashchepkov I, Logvinova A, Spetsius Z and Stegnitsky Y., 2015. Monomineral Mantle
 658 Elcogite CPx and Garnet Thermobarometry. *Goldschmidt 2015 Abstracts*. A126.
- 659 Bedard, J. H., 2006. A catalytic delamination-driven model for coupled genesis of
 660 Archaean crust and sub-continental lithospheric mantle. *Geochimica et Cosmochimica Acta* 70,

- 661 1188 -1214..
- 662 Blundy, J., Wood, B., 1994. Prediction of crystal-melt partition-coefficients from elastic-
663 moduli. *Nature* 372, 452–454.
- 664 Bussweiler, Y., Foley, S.F., Prelević, D., Jacob D.E., 2015. The olivine macrocryst
665 problem: New insights from minor and trace element. *Lithos* 220, 238-252.
- 666 Boyd, F.R., Pokhilenko, N.P., Pearson, D.G., Mertzman S.A., Sobolev, N.V., Finger,
667 L.W., 1997. Composition of the Siberian cratonic mantle: evidence from Udachnaya peridotite
668 xenoliths. *Contributions Mineralogy and Petrology* 128, 228-246.
- 669 Boyd, F.R., 1973. A pyroxene geotherm. *Geochimica et Cosmochimica Acta* 37, 2533-
670 2546.
- 671 Brett, R.C., Russell, J.K., Andrews, G.D.M., Jones, T.J., 2015. The ascent of kimberlite:
672 Insights from olivine. *Earth and Planetary Science Letters* 424, 119–131.
- 673 Burgess, S.R., Harte, B., 2004. Tracing lithosphere evolution through the analysis of
674 heterogeneous G9-G10 garnets in peridotite xenoliths, II: REE chemistry. *Journal of Petrology*
675 45, 609-634.
- 676 Brey, G.P., Kohler, T., 1990. Geothermobarometry in four-phase lherzolites. II. New
677 thermobarometers, and practical assessment of existing thermobarometers. *Journal of Petrology*
678 31, 1353-1378.
- 679 Bussweiler, B., Foley, S.F., Prelević, D., Jacob, D.E., 2014. The olivine macrocryst
680 problem: New insights from minor and trace element compositions of olivine from Lac de Gras
681 kimberlites, Canada. *Lithos* 220, 238–252.
- 682 Cas, R.A.F., Porritt, L., Pittari, A., Hayman, P.C., 2008. A new approach to kimberlite
683 terminology using a revised general approach to the nomenclature of all volcanic rocks and
684 deposits: descriptive to genetic. *J. Volcanol. Journal of Volcanology and Geothermal Research*
685 174, 226–240.
- 686 Clarke, D.B., Mackay, R.M., 1990. An Ilmenite-Garnet-Clinopyroxene nodule from
687 Matsoku: Evidence of Oxide-Rich liquid Immiscibility in Kimberlites? *Canadian Mineralogist*
688 28, 229-239.
- 689 Day H.W., 2012. A revised diamond-graphite transition curve. *American Mineralogist*,
690 97, 52–62.
- 691 DePaolo D.J., 1981. Trace element and isotopic effects of combined wall rock
692 assimilation and fractional crystallization. *Earth Planetary Science Letters* 53, 189-202.
- 693 Doucet, L. S., Peslier, A.H., Ionov, D.A., Brandon, A.D., Golovin, A.V., Goncharov,
694 A.G., Ashchepkov, I.V., 2014. High water contents in the Siberian cratonic mantle linked to

- 695 metasomatism: An FTIR study of Udachnaya peridotite xenoliths. *Geochimica et Cosmochimica*
696 *Acta* 137, 159-187.
- 697 Evans, T.M., O'Neill, C., Tuff, H. St, J., 2008. The influence of melt composition on the
698 partitioning of REEs, Y, Sc, Zr and Al between forsterite and melt in the system CMAS.
699 *Geochim. Cosmochim. Acta* 72, 5708–5721.
- 700 Finnerty, A.A., Boyd, F.R. 1984. Evaluation of thermobarometers for garnet peridotites
701 *Geochimica et Cosmochimica Acta*, 48, 15–27.
- 702 Foley, S.F., Yaxley, G.M., Rosenthal, A., Buhre, S., Kiseeva, E.S., Rapp, R.P., Jacob,
703 D.E., 2009. The composition of near-solidus melts of peridotite in the presence of CO₂ and H₂O
704 between 40 and 60 kbar. *Lithos* 112, 274-283.
- 705 Fulmer, E.C., Nebel, O.P., van Westrenen E., 2010. High-precision high field strength
706 element partitioning between garnet, amphibole and alkaline melt from Kakanui, New Zealand.
707 *Geochimica et Cosmochimica Acta* 74, 2741-2759.
- 708 Genshaft, Yu.S., Ilupin, I.P., 1987. Deep Seated Paragenesis of Ilmenite In The
709 Kimberlite of Yakutia. In: *Studies of Ultra-Basic Minerals*. Moscow. IFZ OF AS USSR.25-68
710 (in Russian).
- 711 Gibson, S.A., Malarkey, J., Day, J.A., 2008. Melt depletion and enrichment beneath the
712 western Kaapvaal Craton: evidence from Finsch peridotite xenoliths. *Journal of Petrology* 49,
713 1817–1852.
- 714 Goncharov, A. G., Ionov, D. A., Doucet, L. S., Pokhilenko, L. N., 2012. Thermal state,
715 oxygen fugacity and C-O-H fluid speciation in cratonic lithospheric mantle: New data on
716 peridotite xenoliths from the Udachnaya kimberlite, Siberia. *Earth and Planetary Science Letters*
717 357, 99-110.
- 718 Gregoire, M., Bell, D. R., Le Roex, A. P., 2002. Trace element geochemistry of
719 phlogopite-rich mafic mantle xenoliths: their classification and their relationship to phlogopite-
720 bearing peridotites and kimberlites revisited. *Contributions to Mineralogy and Petrology* 142,
721 603 -625.
- 722 Green, T.H., Blundy, J.D., Adam, J., Yaxley, G.M., 2000. SIMS determination of trace
723 element partition coefficients between garnet, clinopyroxene and hydrous basaltic liquids at 2–
724 7.5 GPa and 1080–1200°C. *Lithos* 53, 165-187.
- 725 Griffin, W. L., Ryan, C. G., Kaminsky, F. V., O'Reilly, S. Y., Natapov, L. M., Win, T. T.,
726 Kinny, P.D., Ilupin, I. P., 1999a. The Siberian lithosphere traverse: Mantle terranes and the
727 assembly of the Siberian Craton. *Tectonophysics* 310, 1-35.
- 728 Griffin, W. L., O'Reilly, S.Y., Afonso, J.C., Begg, G.C., 2009. The Composition and

- 729 Evolution of Lithospheric Mantle: A Reevaluation and Its Tectonic Implications, *Journal of*
730 *Petrology* 50, 1185–1204
- 731 Griffin, W.L., Spetsius, Z.V., Pearson, N.J., O'Reilly, S.Y. 2002. In-situ Re-Os analysis
732 of sulfide inclusions in kimberlite olivine: New constraints on depletion events in the Siberian
733 lithospheric mantle. *Geochemistry, Geophysics, Geosystems*, 3, (11), 1069,
734 doi:10.1029/2001GC000287.
- 735 Haggerty, S.E. 1975. The chemistry and genesis of opaque minerals in kimberlite. *Physics*
736 *and chemistry of the Earth*. New York 9, 227-243.
- 737 Hammouda, T., Keshav, S. 2015. Melting in the mantle in the presence of carbon: Review
738 of experiments and discussion on the origin of carbonatites. *Chemical Geology* 418, 171-188.
- 739 Hart, S. R., Dunn, T., 1993. Experimental cpx/melt partitioning of 24 trace elements.
740 *Contributions to Mineralogy and Petrology* 113, 1-8.
- 741 Harte, B., Kirkley, M.B., 1997. Partitioning of trace elements between clinopyroxene and
742 garnet: data from mantle eclogites. *Chemical Geology* 136, 1-24.
- 743 Hauri, E.H., Wagner, T.P., Grove, T.L., 1994. Experimental and natural partitioning of
744 Th, U, Pb and other trace elements between garnet, clinopyroxene and basaltic melts. *Chemical*
745 *Geology* 117, 149–166.
- 746 Höfer, H.E., Lazarov, M., Brey, G.P., Woodland, A.B., 2009. Oxygen fugacity of the
747 metasomatizing melt in a polymict peridotite from Kimberley. *Lithos* 112S, 1150–1154
- 748 Giuliani, A., Kamenetsky, V.S., Kendrick, M.A., Phillips, D., Wyatt, B.A., Maas, R.,
749 2013. Oxide, sulphide and carbonate minerals in a mantle polymict breccia: Metasomatism by
750 proto-kimberlite magmas, and relationship to the kimberlite megacrystic suite. *Chemical*
751 *Geology*, 353, 4-18.
- 752 Howarth, G., H. Barry, P.H., Pernet-Fisher, J.F., Baziotis, I. P., Pokhilenko, N.P.,
753 Pokhilenko, L.N., Bodnar, R.J., Taylor, L.A., Agashev, A.M., 2014. Superplume metasomatism:
754 Evidence from Siberian mantle xenoliths. *Lithos* 184–187, 209-224.
- 755 Horn, I., Foley, S.F., Jackson, S.E., Jenner, G.A., 1994. Experimentally determined
756 partitioning of high field strength- and selected transition elements between spinel and basaltic
757 melt. *Chemical Geology* 117, 193–218.
- 758 New Diamond Fields Explored by ALROSA May Turn Into Possible Sources of Reserve
759 Growth. Experet reports -2012. In: Rough and Polished, [http://www.rough-](http://www.rough-polished.com/en/expertise/61434.html)
760 [polished.com/en/expertise/61434.html](http://www.rough-polished.com/en/expertise/61434.html)
- 761 Ionov, D.A., Doucet, L.S., Ashchepkov I.V. 2010. Composition of the Lithospheric
762 Mantle in the Siberian Craton: New Constraints from Fresh Peridotites in the Udachnaya-East
763 Kimberlite. *Journal of Petrology* 51, 2177-2210.

- 764 Ionov, D.A., Bénard, A., Plechov, P.Yu., Shcherbakov, V.D., 2013. Along-arc variations
765 in lithospheric mantle compositions in Kamchatka, Russia: First trace element data on mantle
766 xenoliths from the Klyuchevskoy Group volcanoes. *Journal of Volcanology and Geothermal*
767 *Research* 263, 122–131.
- 768 Ishimaru, S., Arai, S., 2009. Highly silicic glasses in peridotite xenoliths from Avacha
769 volcano, Kamchatka arc; implications for melting and metasomatism within the sub-arc mantle.
770 *Lithos* 107, 93–106.
- 771 Imai, T., Takahashia, E., Suzuki, T., Hirata, T., 2012. Element partitioning between
772 olivine and melt up to 10 GPa: Implications for the effect of pressure. *Physics of the Earth and*
773 *Planetary Interiors* 212, 64–75.
- 774 Karato, S., 2010. Rheology of the Earth's mantle: A historical review. *Gondwana*
775 *Research* 18, 17–45.
- 776 Kargin, A.V., Golubeva, Yu.Yu., Kononova V.A., 2011. Kimberlites of the Daldyn-
777 Alakit region (Yakutia): Spatial distribution of the rocks with different chemical characteristics.
778 *Petrology*. 19 (5), 496–520.
- 779 Katayama, I., Suyama, Y., Ando, S., Komiya, T., 2009. Mineral chemistry and P–T
780 condition of granular and sheared peridotite xenoliths from Kimberley, South Africa: origin of
781 the textural variation in the cratonic mantle. *Lithos* 109, 333–340.
- 782 Kuzyura, A.V., Litvin, Yu.A., Jeffries, T., 2015. Interface partition coefficients of trace
783 elements in carbonate–silicate parental media for diamonds and paragenetic inclusions
784 (experiments at 7.0–8.5 GPa). *Russian Geology and Geophysics* 56, 221–231.
- 785 Khar'kiv, A.D., Zinchuk, N.N., and Kryuchkov, A.I., 1998. *Korennyye mestorozhdeniya*
786 *almazov mira (Primary diamond deposits of the world)*, Moscow: Nedra.
- 787 Kennedy, C.S., Kennedy, G.C., 1976. The equilibrium boundary between graphite and
788 diamond. *Journal of Geophysical Research* 81, 2467–2470.
- 789 Klein-Ben David, O., Pearson, D.G., Nowell G.M., Ottley C., McNeill, J.C.R.,
790 Logvinova, A., Sobolev, N.V., 2014. The sources and time-integrated evolution of diamond-
791 forming fluids – Trace elements and isotopic evidence. *Geochimica et Cosmochimica Acta* 125,
792 146–169.
- 793 Klemme, S., Günther, D., Hametner, K., Prowatke, S., Zack, T., 2006. The partitioning of
794 trace elements between ilmenite, ulvospinel, armalcolite and silicate melts with implications for
795 the early differentiation of the moon. *Chemical Geology* 234, 251–263.
- 796 Kohler, Brey G.P., 1990. Calcium exchange between olivine and clinopyroxene
797 calibrated as a geothermobarometer for natural peridotites from 2 to 60 kb with applications.
798 *Geochemica et Cosmochimica Acta*. 54, 2375–2388.

- 799 Konzett, Y., Wirth, R., Hauzenberger, K., Whitehouse, M., 2013. Two episodes of fluid
800 migration in the Kaapvaal Craton lithospheric mantle associated with Cretaceous kimberlite
801 activity: Evidence from a harzburgite containing a unique assemblage of metasomatic zirconium-
802 phases. *Lithos* 182, 65–184.
- 803 Kopylova, M. G., Nowell, G. M., Pearson, D. G., Markovic, G., 2009. Crystallization of
804 megacrysts from protokimberlitic fluids: Geochemical evidence from high-Cr megacrysts in the
805 Jericho kimberlite. *Lithos* 112, 284–295.
- 806 Kostrovitsky, S. I., Solov'eva, L. V., Yakovlev, D. A., Suvorova, L. F., Sandimirova, G. P.,
807 Travin, A. V., Yudin, D. S., 2013. Kimberlites and megacrystic suite: Isotope-geochemical studies.
808 *Petrology* 21 (2), 127–144.
- 809 Kuzyura, A. V., Litvin, Yu. A., Jeffries, T., 2015. Interface partition coefficients of trace
810 elements in carbonate-silicate parental media for diamonds and paragenetic inclusions
811 (experiments at 7.0–8.5 GPa). *Russian Geology and Geophysics* 56, 221–231.
- 812 Lavrent'ev, Yu. G., Usova, L. V., Kuznetsova, A. I., Letov, S. V., 1987. X-ray spectral
813 quantitative microanalysis of the most important minerals of kimberlites. *Russian Geology and*
814 *Geophysics*, 48 (5), 75–81.
- 815 Logvinova, A. M., Taylor, L. A., Floss, C., Sobolev, N. V., 2005. Geochemistry of multiple
816 diamond inclusions of harzburgitic garnets as examined in situ. *International Geology Review*
817 47, 1223–1233.
- 818 Lavrent'ev, Yu. G., Usova, L. V., Kuznetsova, A. I., Letov, S. V., 1987. X-ray spectral
819 quantitative microanalysis of the most important minerals of kimberlites. *Russian Geology and*
820 *Geophysics* 48 (5), 75–81.
- 821 Lazarov, M., Brey, G. P., Stefan Weyer, S., 2012. Evolution of the South African mantle
822 — A case study of garnet peridotites from the Finsch diamond mine (Kaapvaal craton); part 1:
823 Inter-mineral trace element and isotopic equilibrium. *Lithos* 154, 193–209.
- 824 Laz'ko E. E., Roden M. F., 2003. Garnet Peridotites and Pyroxenites in The
825 Subcontinental Lithosphere of the Central Part of Siberian Craton (Xenoliths From The Mir
826 Pipe) Problems of Prediction, Prospection and Investigation of the Deposits of the Ore and
827 Mineral Resources at the Boundary of XXI Century. Voronezh.. Voronezh State University. pp.
828 307–317 (in Russian)
- 829 Logvinova, A. M., Taylor, L. A., Floss, C., Sobolev, N. V., 2005. Geochemistry of multiple
830 diamond inclusions of harzburgitic garnets as examined in situ. *International Geology Review*
831 47, 1223–1233.
- 832 McCammon, C. A., Griffin, W. L., Shee, S. R., O'Neill, H. S. C., 2001. Oxidation during
833 metasomatism in ultramafic xenoliths from the Wesselton kimberlite, South Africa: implications

- 834 for the survival of diamond. *Contributions Mineralogy and Petrology* 141, 287–296.
- 835 McCammon, C.A., Kopylova, M.G., 2004. A redox profile of the Slave mantle and
836 oxygen fugacity control in the cratonic mantle. *Contributions to Mineralogy and Petrology* 148,
837 55–668.
- 838 McDonough, W.F., Sun, S.-S., 1995. The composition of the Earth. *Chemical Geology*
839 120, 223–253.
- 840 Mitchell, R.H., 1995. *Kimberlites, Orangeites and Related Rocks*. Plenum Press, New
841 York. 410 pp.
- 842 McGregor I.D., 1974. The system MgO- SiO₂-Al₂O₃: solubility of Al₂O₃ in enstatite for
843 spinel and garnet peridotite compositions. *American Mineralogist* 59, 110–119.
- 844 Moore, A.E., Lock, N.P., 2001. The origin of mantle-derived megacrysts and sheared
845 peridotite evidence from kimberlites in the northern Lesotho—Orange Free State (South Africa)
846 and Botswana pipe clusters. *South Africa Journal of Geology* 104, 23–38.
- 847 Moore, A., Belousova, E., 2005. Crystallization of Cr-poor and Cr-rich megacryst suites
848 from the host kimberlite magma: implications for mantle structure and the generation of
849 kimberlite magmas. *Contributions to Mineralogy and Petrology* 49, 462–481.
- 850 Nickel, K.G., 1989. Garnet-pyroxene Equilibria in the System SMACCR (SiO₂-MgO-
851 Al₂O₃-CaO-Cr₂O₃): the Cr-geobarometer. In Ross, J. (ed.): *Kimberlites and Related Rocks, Their*
852 *Mantle/Crust Setting, Diamonds and Diamond Exploration*. Vol.2. Proc. 4th Int. Kimberlite
853 Conf. /Geol. Soc. Aus. Spec. Publ., 14, 901–912.
- 854 Nimis P., Taylor W., 2000. Single clinopyroxene thermobarometry for garnet peridotites.
855 Part I. Calibration and testing of a Cr-in-Cpx barometer and an enstatite-in-Cpx thermometer.
856 *Contributions to Mineralogy and Petrology* 139, 541–554.
- 857 Nimis P., Zanetti A., Dencker I., Sobolev N.V., 2009. Major and trace element
858 composition of chromian diopsides from the Zagadochnaya kimberlite (Yakutia, Russia):
859 Metasomatic processes, thermobarometry and diamond potential. *Lithos* 112, 397–412.
- 860 O'Neill, H. St. C., Wall, V. J., 1987. The olivine orthopyroxene-spinel oxygen
861 geobarometer, the nickel precipitation curve, and the oxygen fugacity of the Earth's upper
862 mantle. *Journal of Petrology* 28, 1169–1191.
- 863 O'Neill, H.St.C, Wood B.J., 1979. An experimental study of Fe-Mg- partitioning
864 between garnet and olivine and its calibration as a geothermometer. *Contributions to Mineralogy*
865 *and Petrology* 70, 59–70.
- 866 Pearson, D.G. and Wittig, N., 2014. The formation and evolution of cratonic mantle
867 lithosphere—Evidence from mantle xenoliths. *Treatise on Geochemistry* 2, 255-292.

- 868 Pernet-Fisher, J.F., Howarth, G.H., Liu, Y., Barry, P.H., Carmody, L., Valley, J.W.,
869 Bodnar, R.J., Spetsius, Z.V., Taylor L.A., 2014. Komsomolskaya diamondiferous eclogites:
870 evidence for oceanic crustal protoliths. *Contributions to Mineralogy and Petrology* 167, 1–17.
- 871 Peslier, A.H., Woodland, A.B., Bell, D. R., Lazarov, M., 2010. Olivine water contents in
872 the continental lithosphere and the longevity of cratons. *Nature* 467, 78–81.
- 873 Pokhilenko, N. P., Sobolev, N.V., Kuligin, S. S., Shimizu, N., 1999. Peculiarities of
874 distribution of pyroxenite paragenesis garnets in Yakutian kimberlites and some aspects of the
875 evolution of the Siberian craton lithospheric mantle. *Proceedings of the VII International*
876 *Kimberlite Conference. The P.H. Nixon volume.* 690–707.
- 877 Pokhilenko, N.P., Pearson, D.G., Boyd, F.R., Sobolev, N.V., 1991. Megacrystalline
878 dunites: sources of Siberian diamonds. *Carnegie Institute Washington. Yearbook* 90, 11–18.
- 879 Pokhilenko, N. P., Sobolev, N.V., Kuligin, S. S., Shimizu, N., 1999. Peculiarities of
880 distribution of pyroxenite paragenesis garnets in Yakutian kimberlites and some aspects of the
881 evolution of the Siberian craton lithospheric mantle. *Proceedings of the VII International*
882 *Kimberlite Conference. The P.H. Nixon volume.* 690–707.
- 883 Pokhilenko, N. P., Sobolev N.V., Sobolev V.S. and Lavrentiev Y.G., 1976. Xenoliths of
884 diamond bearing ilmenite-pyroxene lherzolites from the kimberlite pipe Udachnaya (Yakutia).
885 *Doklady AN SSSR.* 231, 438–442.
- 886 Pokhilenko, N.P., Agashev, A.M., Litasov, K.D., Pokhilenko, L.N., 2015. Carbonatite
887 metasomatism of peridotite lithospheric mantle: implications for diamond formation and
888 carbonatite-kimberlite magmatism. *Russian Geology and Geophysics* 56, 280–295.
- 889 Rodionov, A.S., Amshinsky A.N., Pokhilenko, N P., 1988. Ilmenite – Pyrope wehrlite –
890 are the new type of paragenesis in xenoliths from kimberlite. *Russian Geol. Geophys.* 19/7, 53–
891 57.
- 892 Rodionov, A S., Amshinsky., Pokhilenko, N P., Sobolev, N.V., 1984. Comparative
893 description of the main minerals in the concentrate of two varieties of kimberlites in Dal'nyaya
894 pipe (Yakutia). *Russian Geol. Geophys.* 17, 38–50.
- 895 Rodionov, A.S., Sobolev, N.V., Pokhilenko, N.P., Suddaby, P., Amshinsky, A.N., 1991.
896 Ilmenite-bearing peridotites and megacrysts from Dalnyaya kimberlite pipe, Yakutia. *Fifth*
897 *International Kimberlite Conference: Extended abstracts, United States,* 339–341.
- 898 Rudnick, R.L., McDonough, W.F., O'Connell R.J., 1998. Thermal structure, thickness
899 and composition of continental lithosphere. *Chemical Geology* 145, 395–411.
- 900 Sazonova, L.V., Nosova, A.A., Kargin, A.V., Borisovskiy, S.E., Tretyachenko, V.V.,
901 Abazova, Z.M., Griban' Yu.G., 2015. Olivine from the Pionerskaya and V. Grib kimberlite

902 pipes, Arkhangelsk diamond province, Russia: Types, composition, and origin. *Petrology* 23,
903 227–258.

904 Smelov, A.P., Zaitsev, A.I., 2013. The Age and Localization of Kimberlite Magmatism in
905 the Yakutian Kimberlite Province: Constraints from Isotope Geochronology—An Overview.
906 Pearson D. G. et al. (eds.), *Proceedings of 10th International Kimberlite Conference, Volume 1*,
907 Special Issue of the *Journal of the Geological Society of India*, 225–234.

908 Sobolev, N.V., Lavrent'ev, Y.G., Pokhilenko, N.P., Usova, L.V., 1973. Chrome-Rich
909 Garnets from the Kimberlites of Yakutia and Their Parageneses. *Contributions to Mineralogy*
910 and *Petrology* 40, 39–52.

911 Sobolev, N.V., Logvinova, A.M., Zedgenizov, D.A., Pokhilenko, N.P., Malygina, E.V.,
912 Kuzmin, D.V., Sobolev, A.V., 2009. Petrogenetic significance of minor elements in olivines
913 from diamonds and peridotite xenoliths from kimberlites of Yakutia. *Lithos*, 112S1, 701–713.

914 Sobolev, N.V., Sobolev, A.V., Tomilenko, A.A., Kovyazin, S.V., Batanova, V.G.,
915 Kuz'min, D.V., 2015. Paragenesis and complex zoning of olivine macrocrysts from unaltered
916 kimberlite of the Udachnaya-East pipe, Yakutia: relationship with the kimberlite formation
917 conditions and evolution. *Russian Geology and Geophysics* 56, 260–279.

918 Sobolev, N.V., 1977. Deep-Seated Inclusions in Kimberlites and the Problem of the
919 Composition of the Mantle. *Amer. Geophys. Union, Washington, DC*. 279 pp.

920 Sobolev, N.V., Pokhilenko, N.V., Efimova, E.S., 1984. Xenoliths of diamond bearing
921 peridotites in kimberlites and problem of the diamond origin. *Russian Geology and Geophysics*,
922 25, 63–80.

923

924 Sobolev, N.V., Logvinova, A.M., Zedgenizov, D.A., Pokhilenko, N.P., Malygina, E.V.,
925 Kuzmin, D.V., Sobolev, A.V., 2009. Petrogenetic significance of minor elements in olivines
926 from diamonds and peridotite xenoliths from kimberlites of Yakutia. *Lithos*, 112, 701-713.

927 Sobolev N.V., Kuznetsova, I.K., Zyuzin, N.I., 1968. The petrology of grosspydite
928 xenoliths from the Zagadochnaya kimberlite pipe in Yakutia. *Journal of Petrology* 9, 253–280.

929 Solov'eva, L.V., Yasnygina, T.A., Egorov K.N., 2012. Metasomatic parageneses in deep-
930 seated xenoliths from pipes Udachnaya and Komsomol'skaya-Magnitnaya as indicators of fluid
931 transfer through the mantle lithosphere of the Siberian craton. *Russian Geology and Geophysics*
932 53, 1304–1323.

933 Sobolev N.V., Kuznetsova, I.K., Zyuzin, N.I., 1968. The petrology of grosspydite
934 xenoliths from the Zagadochnaya kimberlite pipe in Yakutia. *Journal of Petrology* 9, 253–280.

- 935 Spetsius, Z.V., 2007. The nature of indicator minerals in kimberlites: a case from the
936 mantle xenoliths studying. Plumes and their sources. Ed. by N.V. Vladykin. Irkutsk. Institute of
937 Geography, 90–108.
- 938 Spetsius, Z.V., Serenko, V.P., 1990. Composition of the Continental Mantle and Low
939 Crust Beneath the Siberian Platform. Moscow, Nauka. 271 pp (in Russian).
- 940 Stachel, T., Luth, R.W., 2015. Diamond formation — Where, when and how? *Lithos* 220,
941 200–220.
- 942 Stagno, V. Frost, D.J., 2010. Carbon speciation in the asthenosphere: experimental
943 measurements of the redox conditions at which carbonate - bearing melts coexist with graphite
944 or diamond in peridotite assemblages. *Earth Planetary Science Letters* 300, 72–84,
- 945 Stagno, V., Ojwang, D.O., McCammon, C.A. Frost, D.J., 2013. The oxidation state of
946 the mantle and the extraction of carbon from Earth's interior. *Nature* 493, 84–88.
- 947 Sun, C., Liang, Y., 2015. A REE-in-garnet–clinopyroxene thermobarometer for eclogites,
948 granulites and garnet peridotites. *Chemical Geology* 393, 79–92.
- 949 Tappe, S., Pearson, D.G., Kjarsgaard, B.A., Nowell, G., Dowall, D., 2013. Mantle
950 transition zone input to kimberlite magmatism near a subduction zone: Origin of anomalous Nd–
951 Hf isotope systematics at Lac de Gras, Canada. *Earth and Planetary Science Letters* 371, 235–
952 251.
- 953 Taylor, W.R., Kammerman, M., Hamilton, R., 1998. New thermometer and oxygen
954 fugacity sensor calibrations for ilmenite and chromian spinel-bearing peridotitic assemblages. 7th
955 International Kimberlite Conference. Extended abstracts. Cape Town. 891–901
- 956 Tappe, S., Pearson, D.G., Kjarsgaard, B.A., Nowell, G., Dowall, D., 2013. Mantle
957 transition zone input to kimberlite magmatism near a subduction zone: Origin of anomalous Nd–
958 Hf isotope systematics at Lac de Gras, Canada. *Earth and Planetary Science Letters* 371, 235–
959 251.
- 960 Taylor, W.R., Kammerman, M., Hamilton, R. 1998. New thermometer and oxygen
961 fugacity sensor calibrations for ilmenite and chromian spinel-bearing peridotitic assemblages. 7th
962 International Kimberlite Conference. Extended abstracts. Cape Town. 891–901
- 963 Tappe, S., Foley, S.F., Jenner, G.A., Heaman L.M., Kjarsgaard B. A., Romer R. L.,
964 Stracke A., Joyce N., Hoefs J., 2006. Genesis of ultramafic lamprophyres and carbonatites at
965 Aillik Bay, Labrador: a consequence of incipient lithospheric thinning beneath the North Atlantic
966 craton *Journal of Petrology* 47, 1261–1315.
- 967 Tuff, J., Gibson, S., 2007. Trace-element partitioning between garnet, clinopyroxene and
968 FE-rich picritic melts at 3 to 7 Gpa. *Contributions to Mineralogy and Petrology* 153, 369–387.

- 969 Walter, M.J., 1998. Melting of Garnet Peridotite and the Origin of Komatiite and
970 Depleted Lithosphere. *Journal of Petrology* 39, 29–60.
- 971 Wang, H., van Hunen, J., Pearson, D.G., 2015. The thinning of subcontinental
972 lithosphere: The roles of plume impact and metasomatic weakening. *Geochemistry, Geophysics,*
973 *Geosystems* 16(4), 1156-1171.
- 974 Wu, C.-M., Zhao, G., 2011. The applicability of garnet–orthopyroxene geobarometry in
975 mantle xenoliths. *Lithos* 125, 1–9.
- 976 Zack, T., Brumm, R., 1998. Ilmenite/liquid partition coefficients of 26 trace elements
977 determined through ilmenite/clinopyroxene partitioning in garnet pyroxenite. In: Gurney, J.J.,
978 Gurney, J.L., Pascoe, M.D., Richardson, S.H. (Eds.), 7th International Kimberlite Conference.
979 In: *Red Roof Design*, Cape Town, 986–988.
- 980 Ziberna, L., Nimis, P., Zanetti, A., Marzoli, A., Sobolev N.V., 2013. Metasomatic
981 Processes in the Central Siberian Cratonic Mantle: Evidence from Garnet Xenocrysts from the
982 Zagadochnaya Kimberlite. *Journal of Petrology* 54, 2379–2409.

983

984 **Figure captions**

985 Fig. 1. Location of Dalnyaya pipe within the YKP and Daldyn-Alakit kimberlite fields in
986 Siberian platform. (A) General scheme of Siberian craton and kimberlite fields. (B) Scheme of
987 the area around Dalnyaya pipe from Google maps.

988

989 Fig. 2. Scanned images of thin sections of mantle xenoliths from Dalnyaya pipe. (A-C) Ilmenite
990 megacrysts with clinopyroxene and polyphase inclusions; (D) low-Cr websterite. E, F:
991 clinopyroxene-rich clusters in garnet lherzolites; (F, G, J) garnet-rich clusters in peridotite; (H, P)
992 orthopyroxene-rich clusters in garnet lherzolites; (L, R) deformed peridotites; (K, N, S)
993 porphyroclastic peridotites; (M, O, W) ilmenite-bearing vein in garnet peridotite; (T)
994 fragmentation of peridotite – and clinopyroxenite by protokimberlite melt; (U) garnet peridotite
995 interacted with melt; (V) garnet harzburgite; (X) coarse garnet dunite

996

997 Fig. 3. Compositions of the pyropes (A) from AKB, (B) PK and (C) peridotitic xenoliths from
998 Dalnyaya pipe. In Cr_2O_3 vs CaO plot, the composition of garnets from Rodionov et al. (1984) are
999 shown by small dots. In addition the analyses of the mineral grains from xenoliths and those
1000 analyzed by ICP are shown by stars (see legend).

1001

1002 Fig.4. Compositions of Cr-diopsides from (A) AKB; (B) PK and (C) peridotitic xenoliths from
1003 Dalnyaya pipe.

1004

1005 Fig. 5. Compositions of chromites in peridotitic xenoliths from Dalnyaya pipe and from (A)AKB
1006 and (B)PK according to Rodionov et al.(1984).

1007

1008 Fig.6. Compositions of ilmenites from AKB (A) and PK (B) from Dalnyaya pipe. In addition the
1009 analyses of the mineral grains from xenoliths and those analyzed by ICP are shown by stars (see
1010 legend).

1011

1012 Fig.7. Compositions of phlogopites from mantle xenoliths from Dalnyaya pipe. Fields of
1013 disseminated and veined phlogopites from Sytykanskaya (Ashchepkov et al., 2015) pipe are also
1014 plotted

1015

1016 Fig.8. Variation diagrams for olivines from mantle xenoliths from Dalnyaya pipe relative to $\text{Fe}^\#$
1017 from the routine EPMA analyses.

1018

1019

1020 Fig.9. Comparison of the Orthopyroxene-based geotherm. (A) Opx T ($^{\circ}\text{C}$) (Brey and Kohler,
 1021 1990) – P (GPa) (McGregor, 1974) and P – T estimates obtained with other combinations of
 1022 thermobarometers; (B) P (GPa) (Brey and Kohler, 1990) – T ($^{\circ}\text{C}$) by Cpx; (C) P (GPa) (Brey and
 1023 Kohler, 1990) and T ($^{\circ}\text{C}$) by Opx. T ($^{\circ}\text{C}$) (Brey and Kohler, 1990) and P (GPa) by (Nickel and
 1024 Green, 1985); (D) P – T by (Nimis and Taylor, 2000); (E) T ($^{\circ}\text{C}$) (Nimis and Taylor, 2000Cor)– P
 1025 (GPa) (Ashchepkov et al., 2015Cpx); (F) T ($^{\circ}\text{C}$) (O’Neil and Wood, 1979 Mono) – P (GPa)
 1026 (Ashchepkov et al., 2015Gar).

1027

1028 Fig. 10. (A) P – T – X – $f(\text{O}_2)$ diagram for minerals from xenoliths found in Dalnyaya pipe
 1029 kimberlite. 140 xenoliths from our collection and some associations from Rodionov and
 1030 colleagues (1983, 1993); (B) P – T – X – $f(\text{O}_2)$ diagram for the minerals from the heavy mineral
 1031 separates of PK; (C) P – T – X – $f(\text{O}_2)$ diagram for the minerals from the heavy mineral separates of
 1032 ABK. Symbols: 1. Opx: T ($^{\circ}\text{C}$) (Brey and Kohler, 1990) vs P (GPa) (McGregor, 1974). 2. Cpx:
 1033 T ($^{\circ}\text{C}$) vs P (GPa) (Nimis and Taylor, 2000); 3. T ($^{\circ}\text{C}$) (Nimis and Taylor, 2000) vs P (GPa)
 1034 (Ashchepkov et al., 2011); 4. same for pyroxenites; 5. The same for pyroxenes analyzed by ICP.
 1035 for garnets: 6. T ($^{\circ}\text{C}$) (O’Neill and Wood, 1979)– P (GPa) (Ashchepkov et al., 2010), Chromite 7.
 1036 T ($^{\circ}\text{C}$) (O’Neill and Webb, 1987)– P (GPa) (Ashchepkov et al., 2010); 8. Ilmenite megacrysts T
 1037 ($^{\circ}\text{C}$) (Taylor et al., 1998) – (Ashchepkov et al., 2010); 9. The same for xenoliths; 10. For
 1038 Olivines $\text{Fe}^{\#}$ – P (GPa) (Ashchepkov et al., 2011) (Cpx associated with Ol); 11. T ($^{\circ}\text{C}$)– P (GPa)
 1039 (Brey and Kohler, 1990). In the P – T plot the approximate the diamond-graphite transition
 1040 Kennedy and Kennedy (1976) is shown. In P – $f(\text{O}_2)$ plot the diamond stability field is after
 1041 Stagno and Frost (2013).

1042

1043 Fig. 11. REE and spider diagrams for minerals from peridotitic xenoliths from the Dalnyaya
 1044 pipe. Normalization to primitive mantle (PM) after McDonough and Sun (1995).

1045

1046 Fig. 12. REE and spider diagrams for ilmenite megacrysts and their clinopyroxene Inclusions(A)
 1047 and the minerals from concentrates of the Dalnyaya pipe(B). Normalization to primitive mantle
 1048 after McDonough and Sun (1995).

1049

1050 Fig. 13. REE and spider diagrams for calculated melts in equilibrium with (A) clinopyroxenes,
 1051 K_D after (Hart and Dunn, 1993); (B) olivines and orthopyroxene, K_D after (Ionov et al., 1995);
 1052 (C) garnets from refertilized peridotites, (D) ilmenite megacrysts and their clinopyroxene

1053 inclusions. The dashed lines represent the range of kimberlite compositions in Dalnyaya pipe
1054 after Kargin et al. (2011). Partition coefficients for clinopyroxenes (Hart and Dunn, 1993), for
1055 garnets (Green et al., 2000) and for ilmenites (Zack and Brumm, 1998; Klemme et al., 2006).
1056 Normalization to primitive mantle after McDonough and Sun (1995).

1057

1058

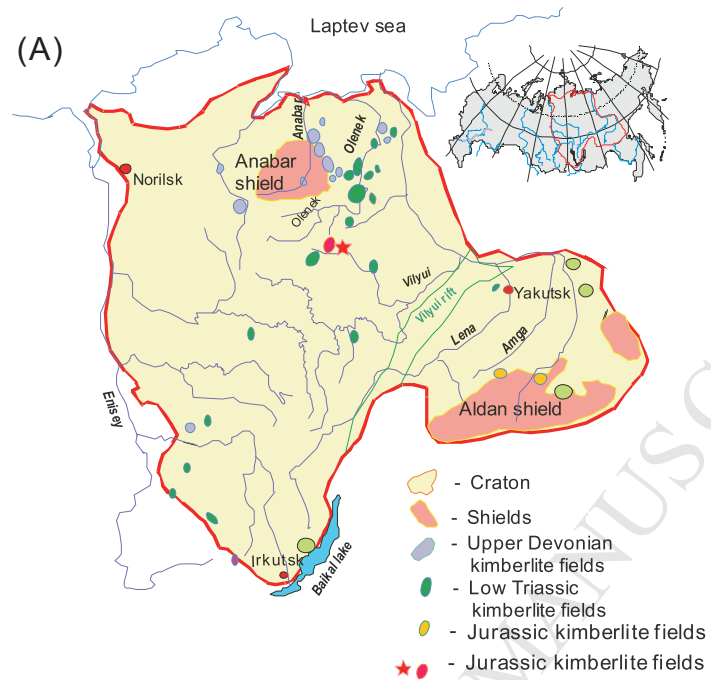
1059 Fig. 14. Partition coefficients determined. (A) Clinopyroxenes /garnet for the relatively
1060 equilibrated associations garnet-clinopyroxenes; (B) clinopyroxenes /ilmenite for the ilmenite-
1061 clinopyroxene intergrowths and calculated ilmenite-melt coefficient for the sample DL175.

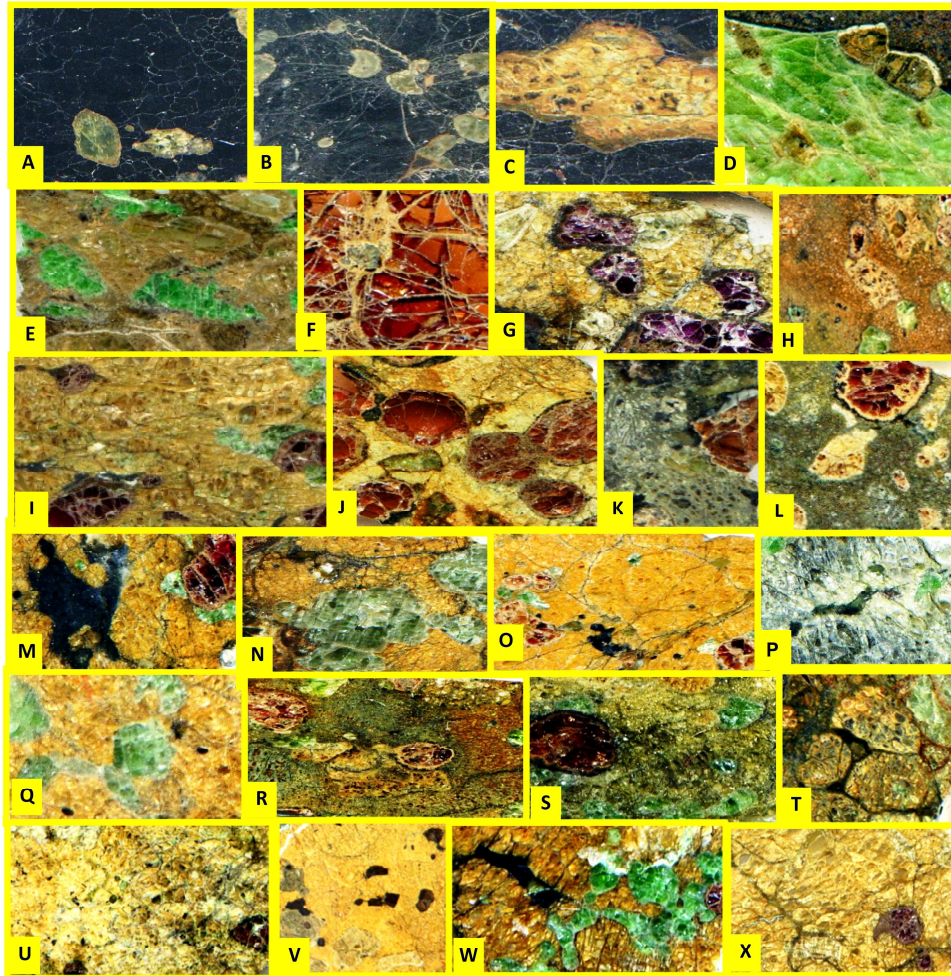
1062 Normalization to primitive mantle after McDonough and Sun (1995).

1063

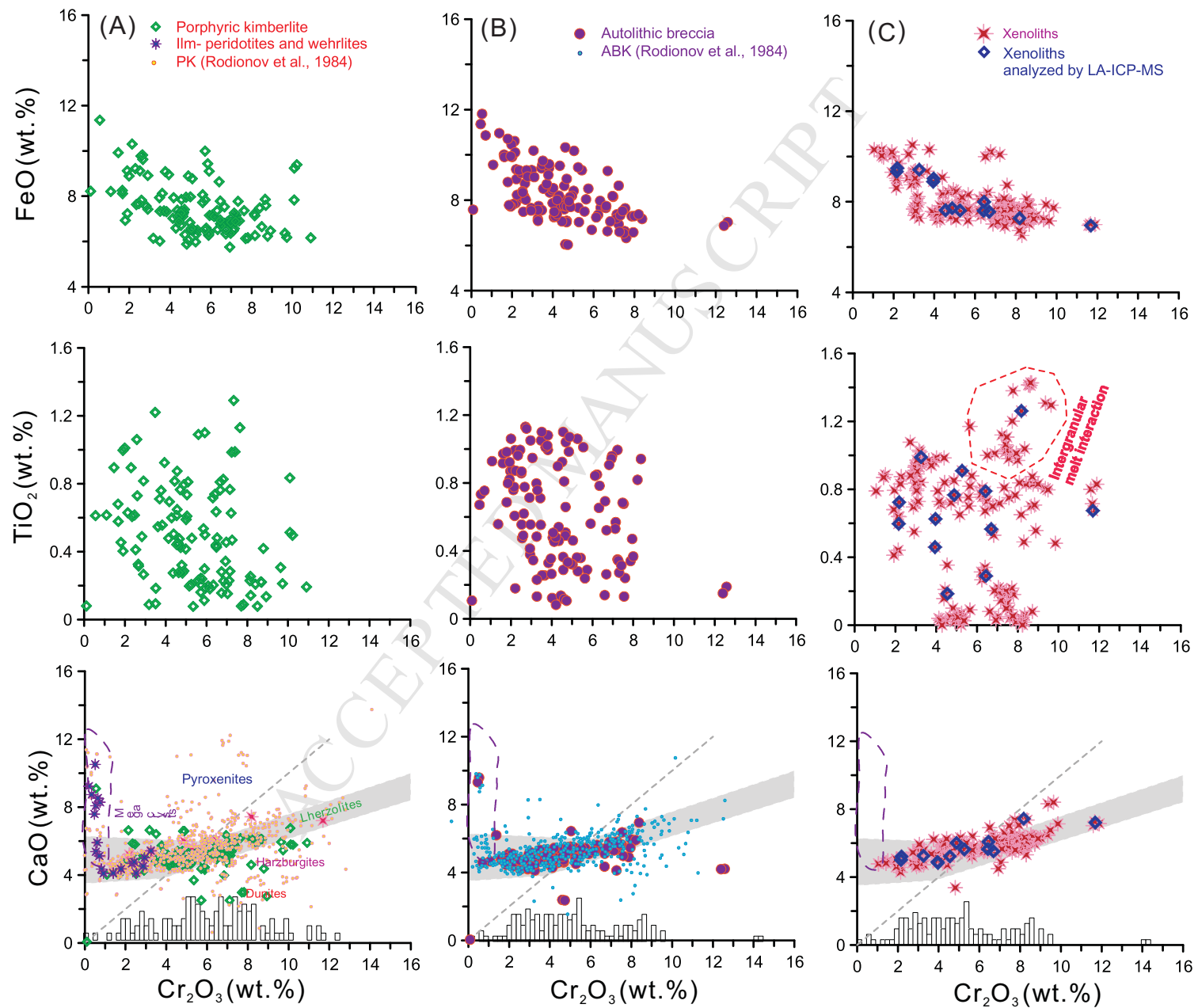
1064 Fig. 15. Different variations of protokimberlite melt evolution (calculated according to AFC
1065 model of DePaolo, 1981) and compositions of the minerals in equilibrium. (A) Gar from melt
1066 assimilating Cpx ($R=0.5$); (B) Cpx from melt assimilating Gar; (C) Cpx from melt assimilating
1067 Opx ($R=0.5$); (D) Gar from melt assimilating Ilm. K_D for Gar/Melt (Green et al., 2000), for Cpx
1068 (Hart and Dunn, 1993). Normalization to primitive mantle after McDonough and Sun (1995).

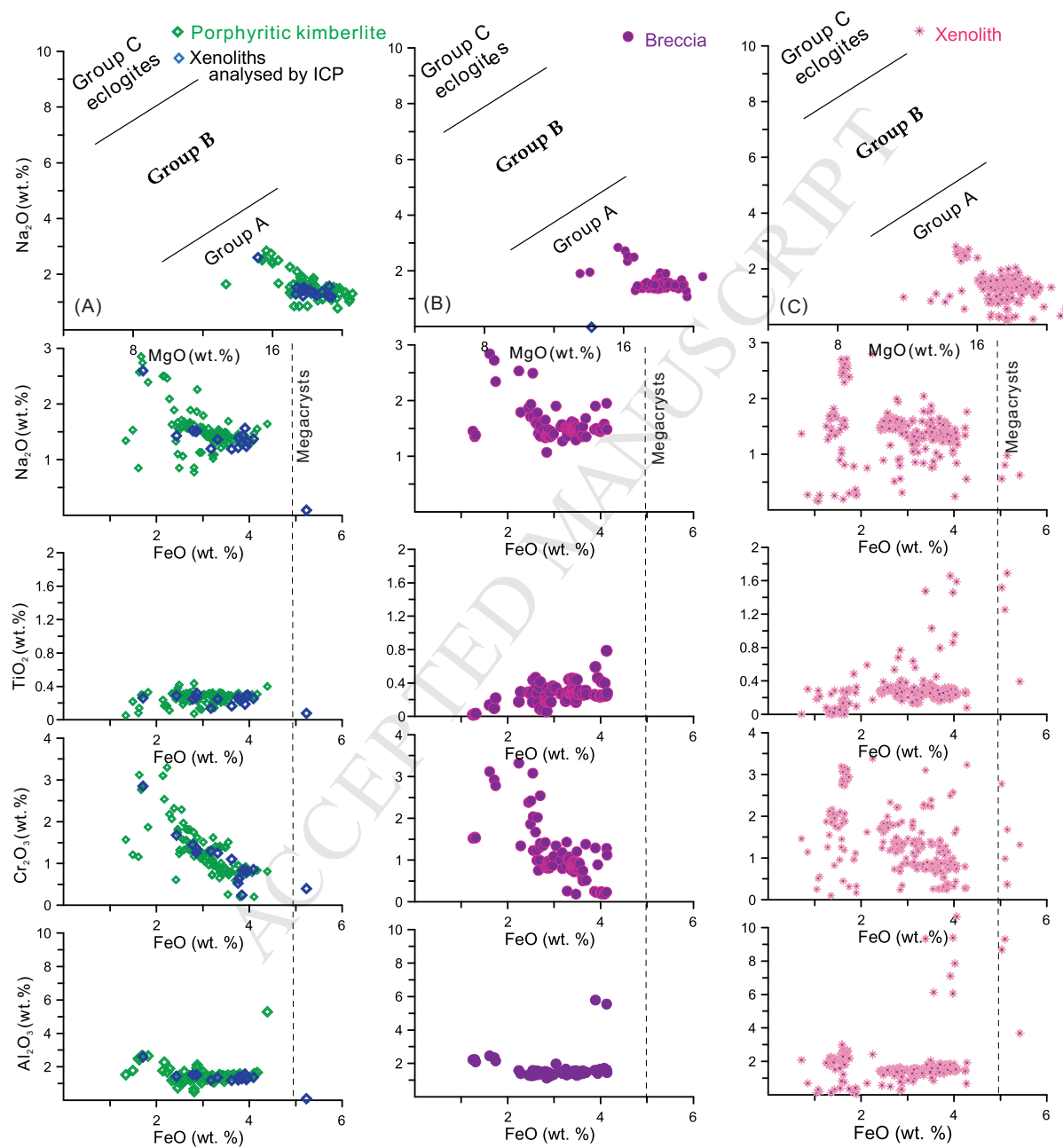
1069

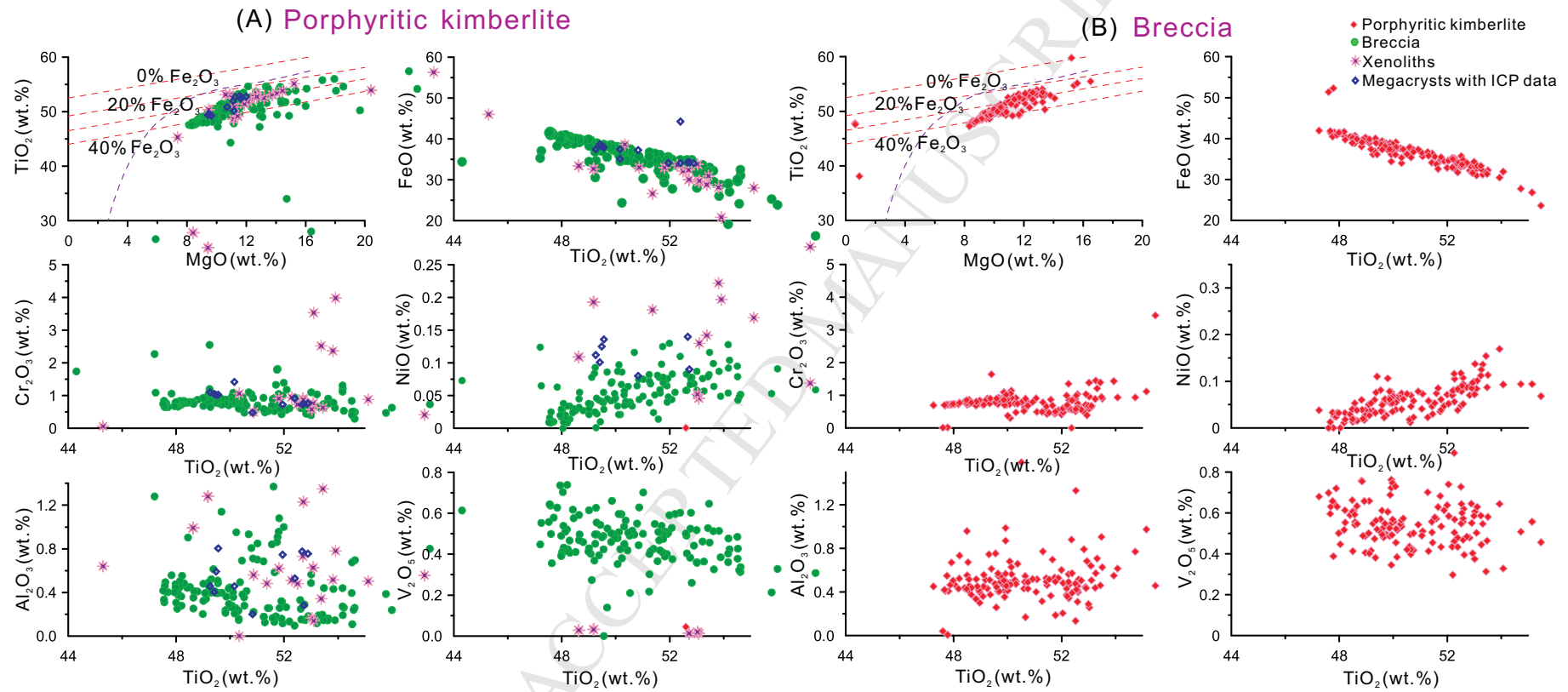


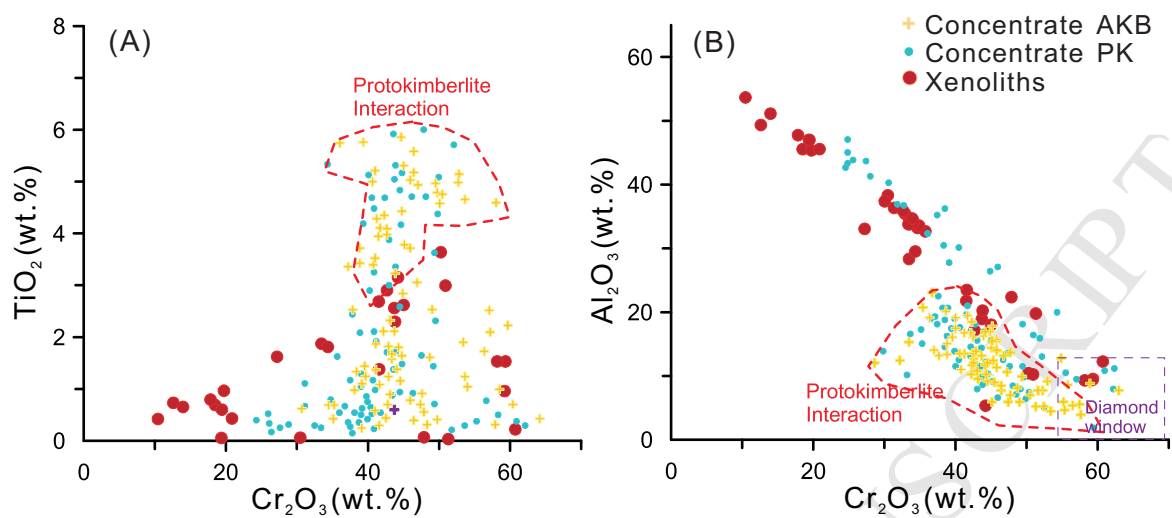


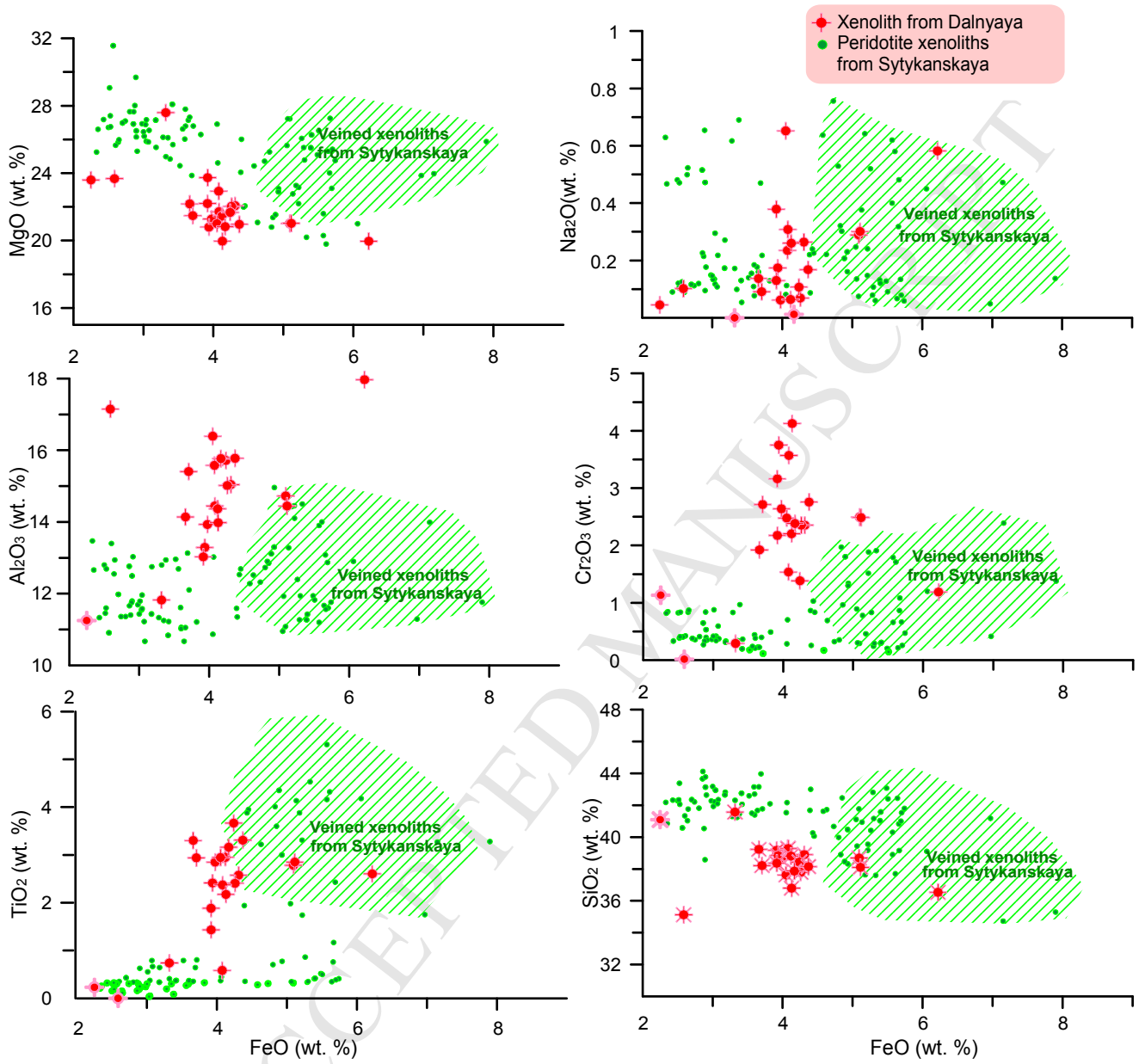
ACCEPTED MANUSCRIPT

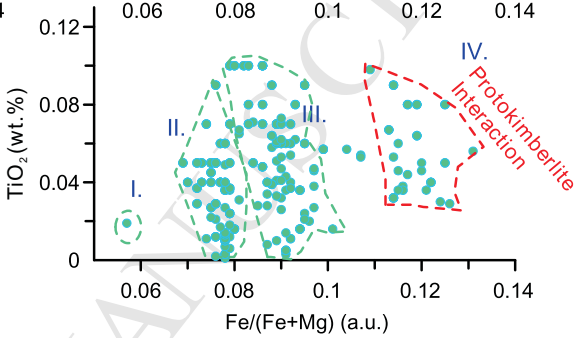
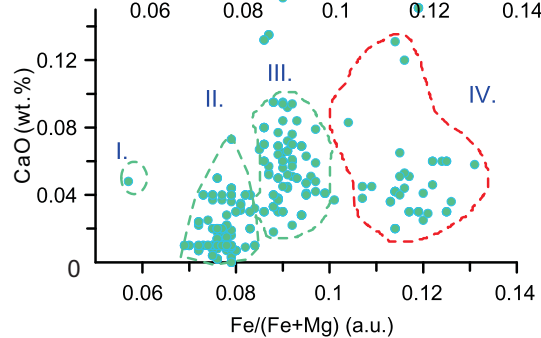
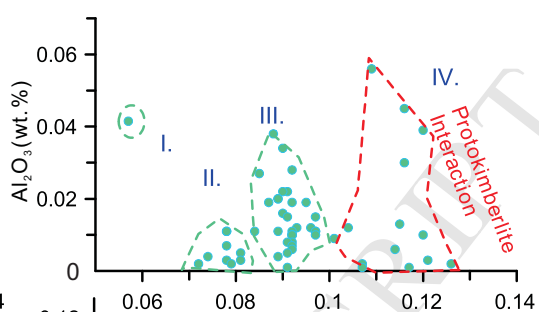
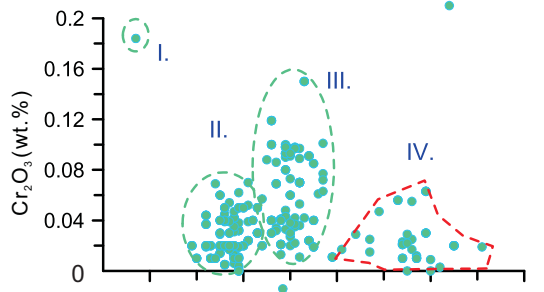
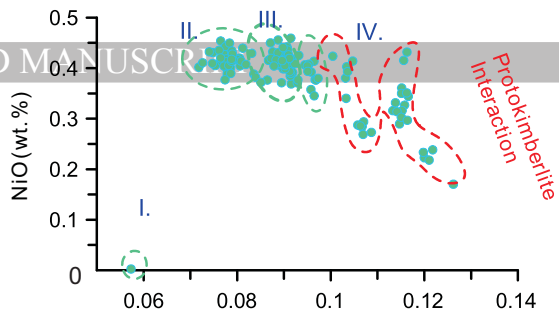
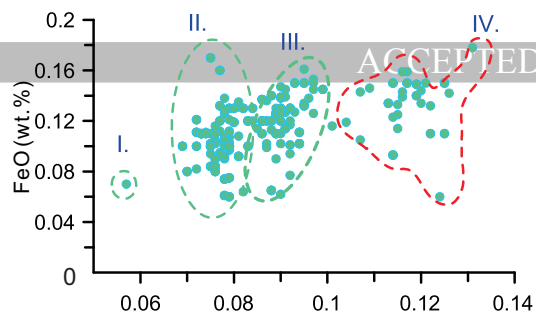




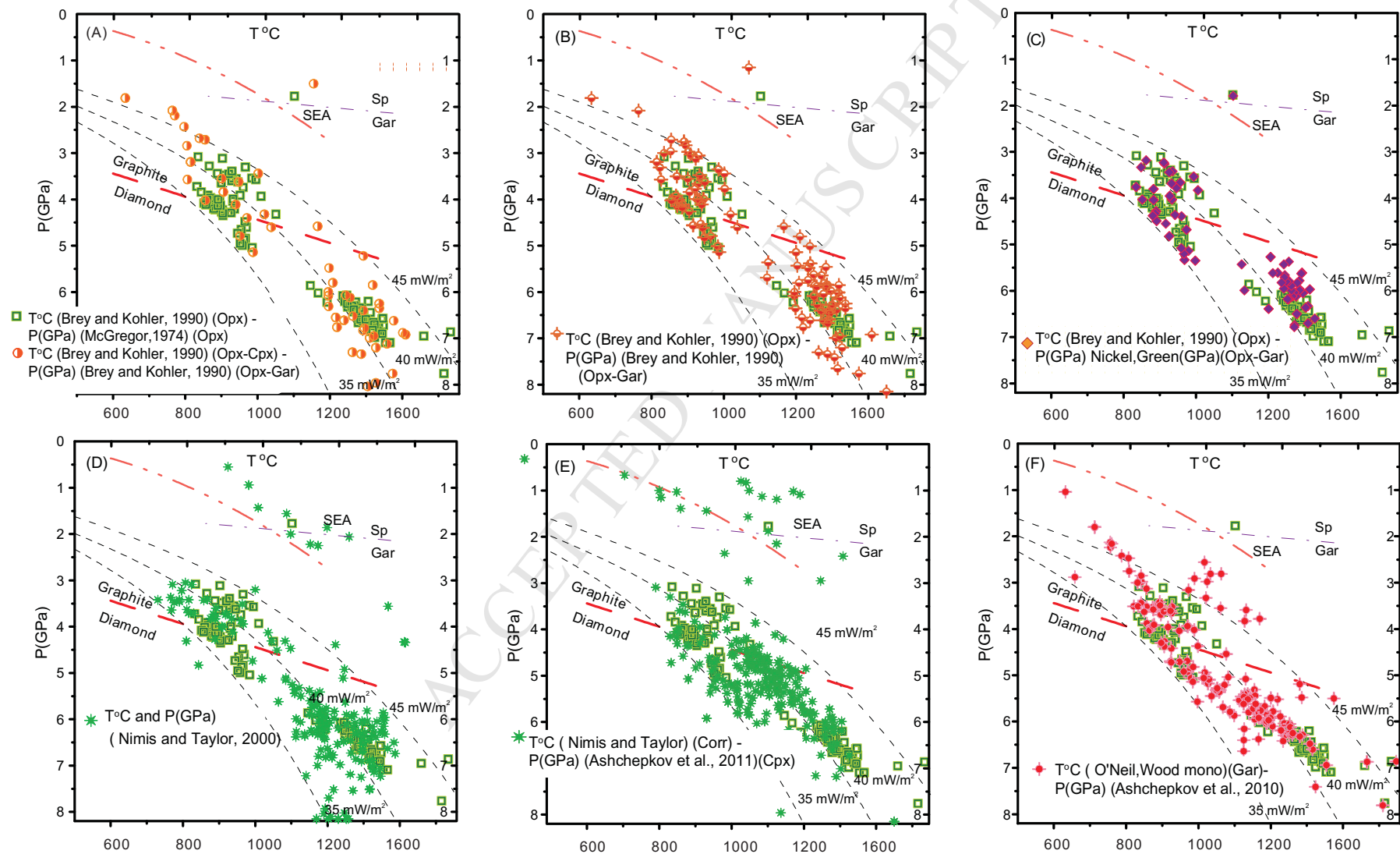


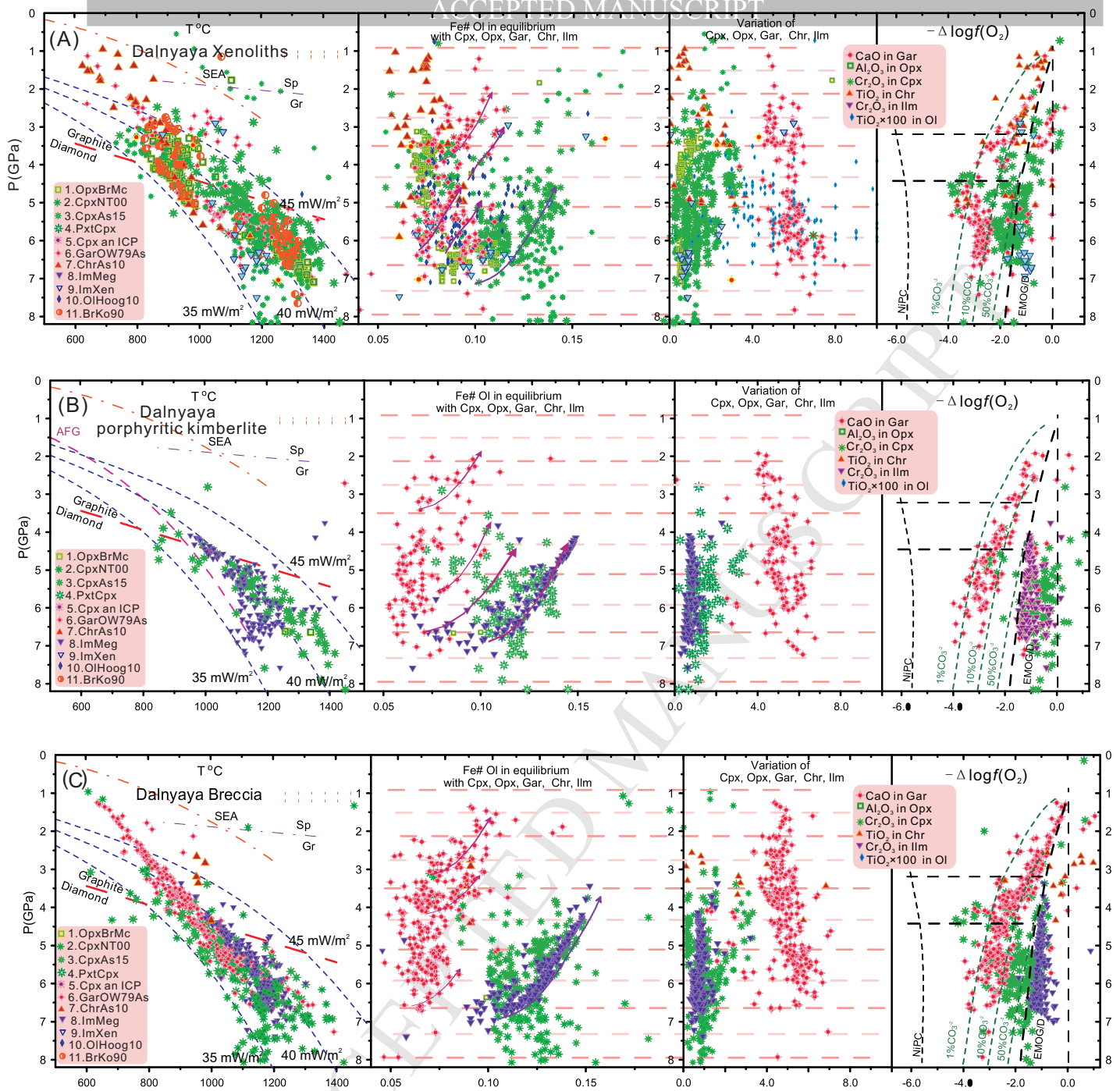






Dalnyaya





Dalnaya all peridotitic minerals analyzed by LA-
ICP-MS in thin sections

Minerals from peridotite xenoliths

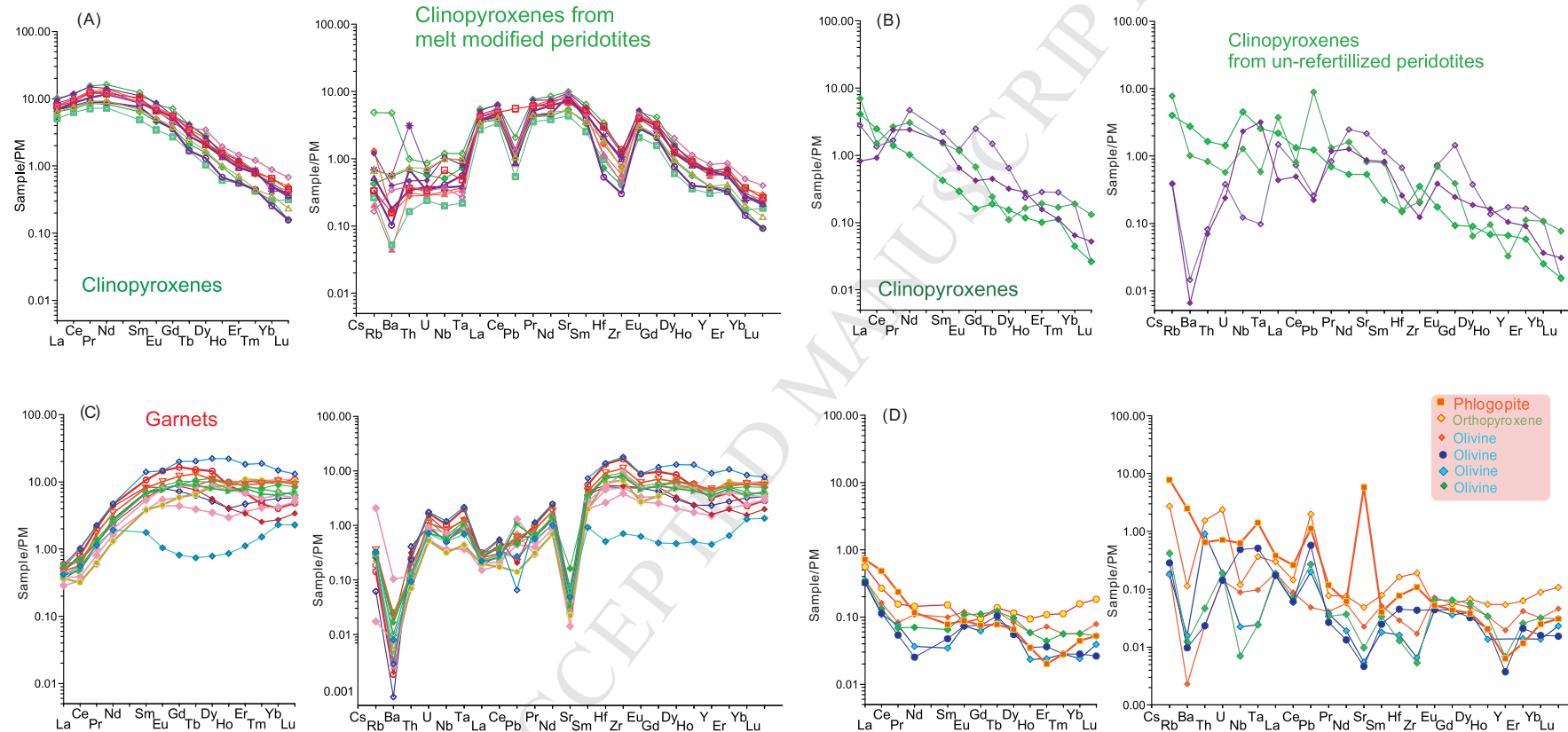
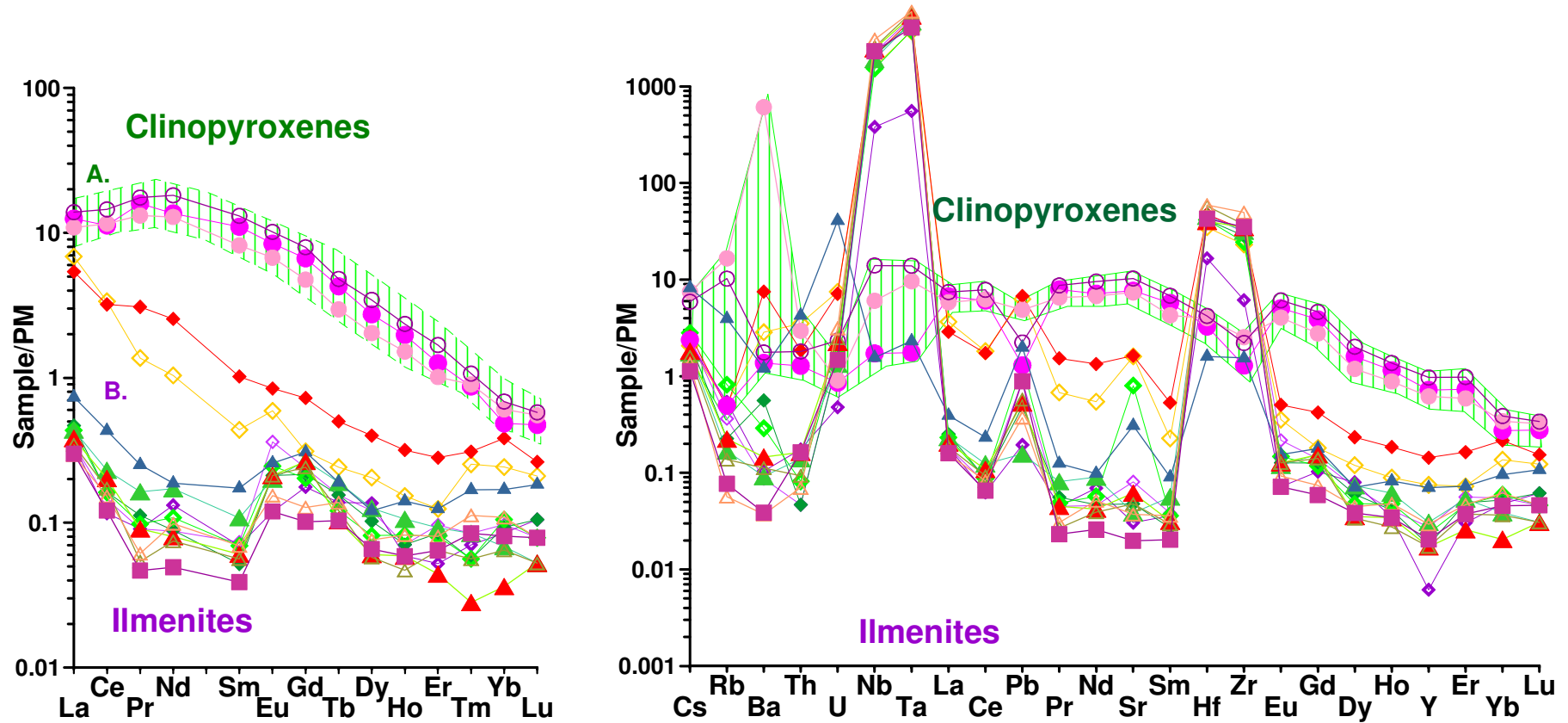
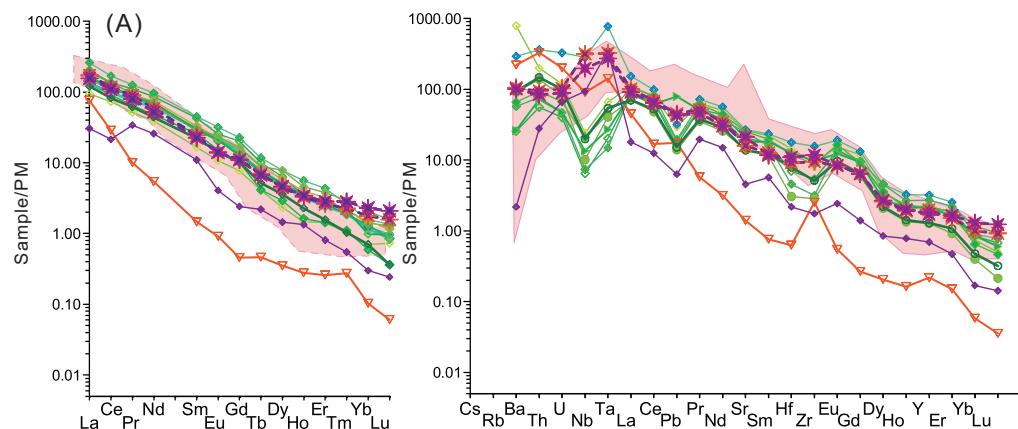


Fig.12

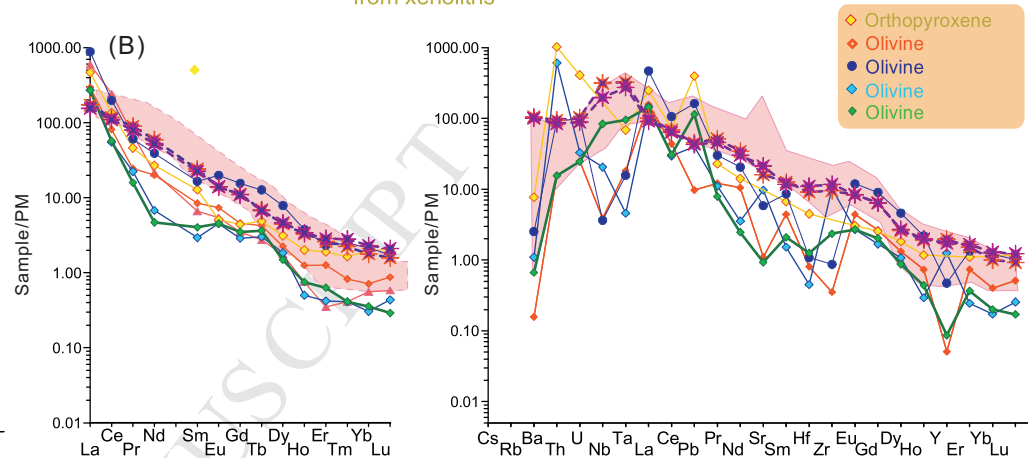
Ilmenite - diopside nodules



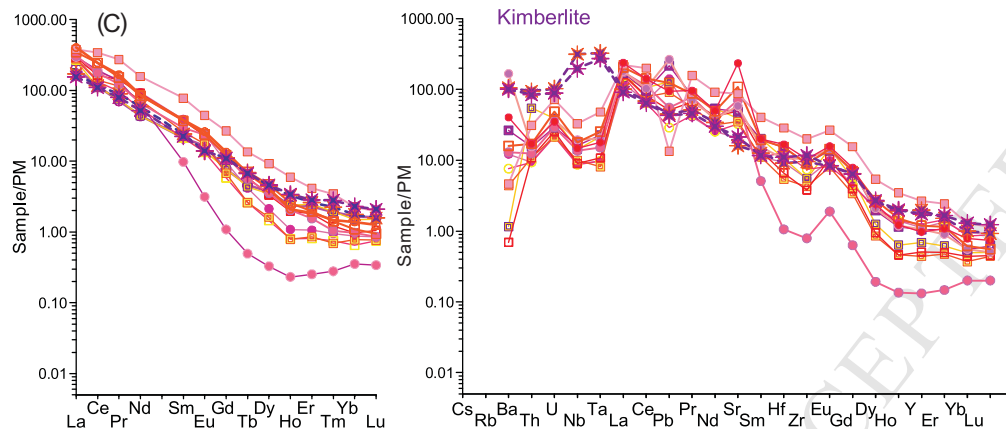
Melts in equilibrium with clinopyroxenes from xenoliths



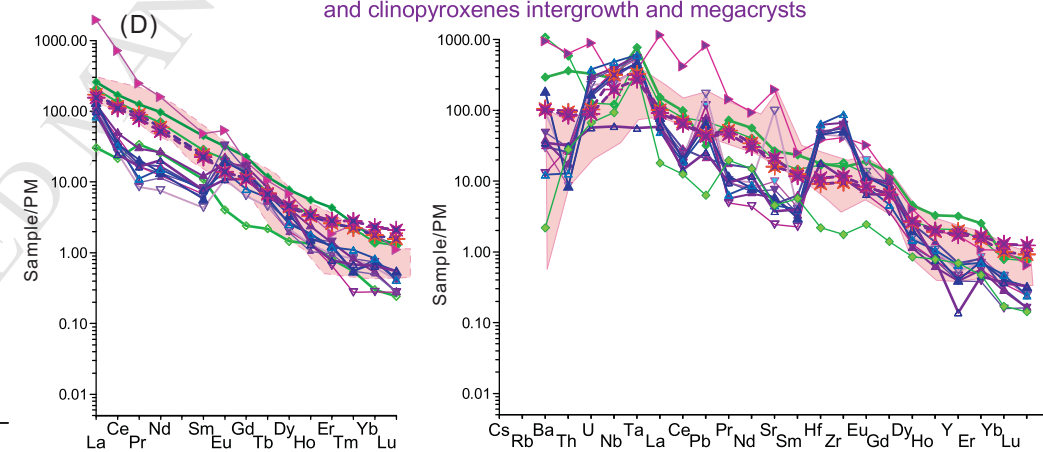
Melts in equilibrium with olivines and orthopyroxenes from xenoliths



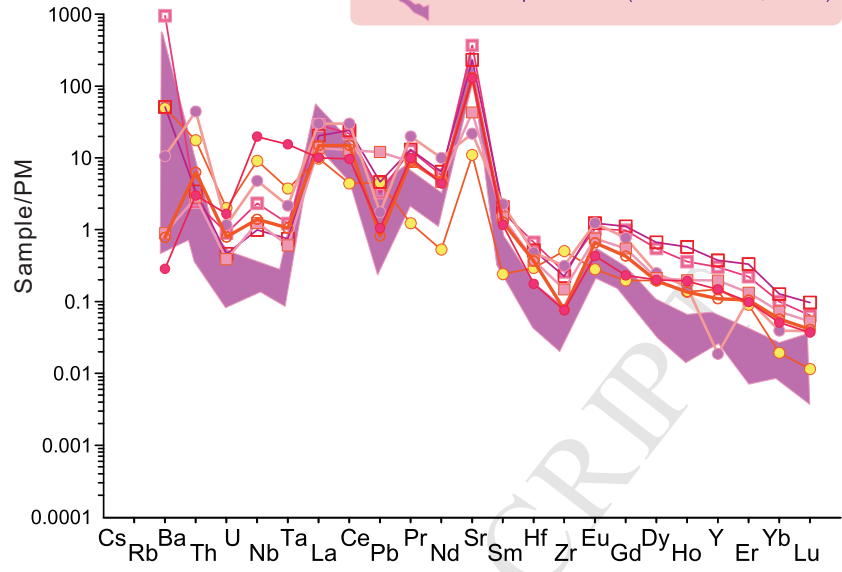
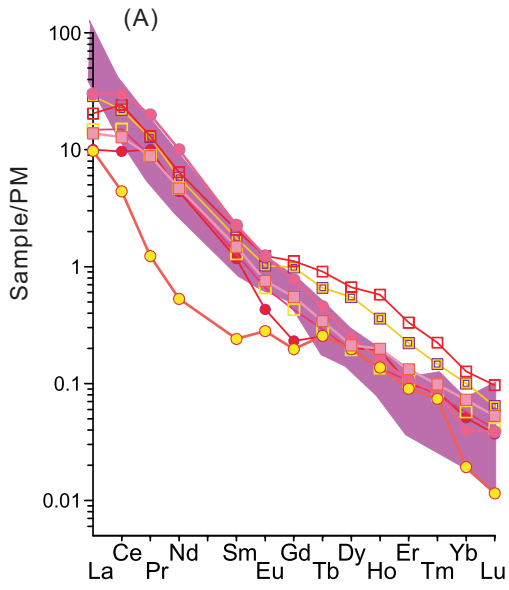
Melts in equilibrium with garnets from xenoliths



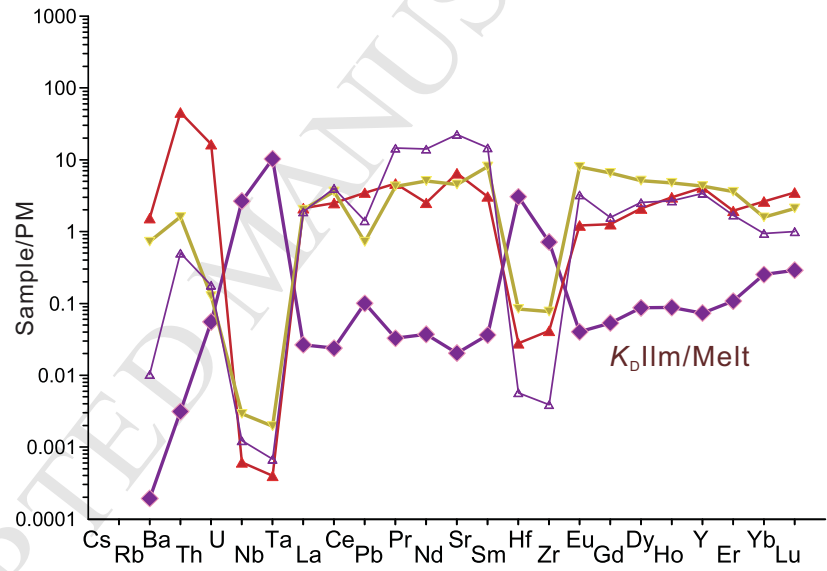
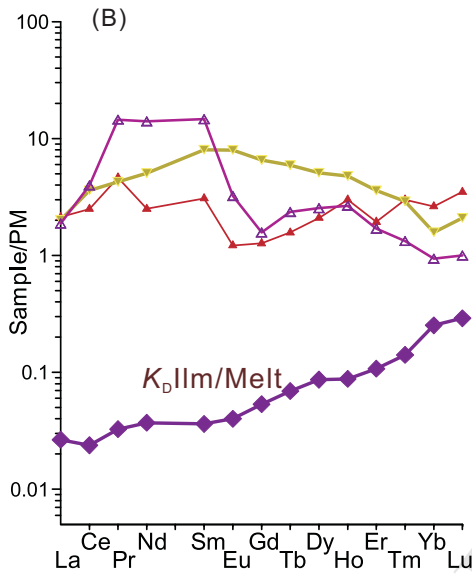
Melts in equilibrium with Ilmenites and clinopyroxenes intergrowth and megacrysts

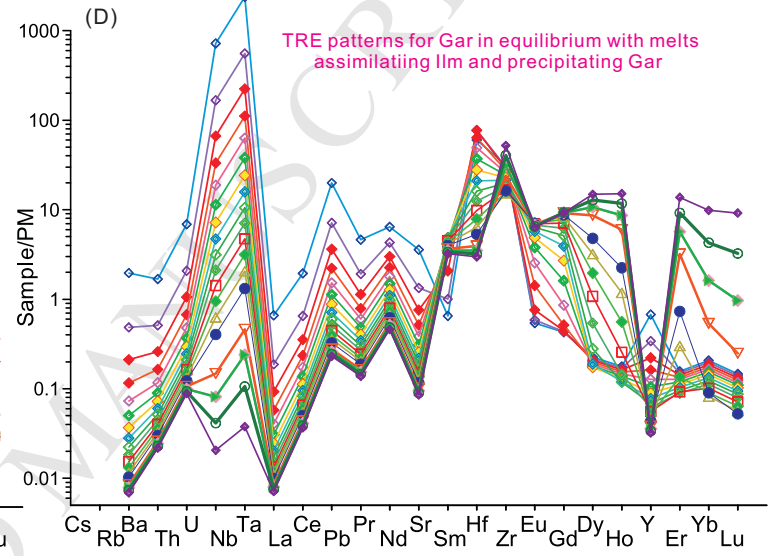
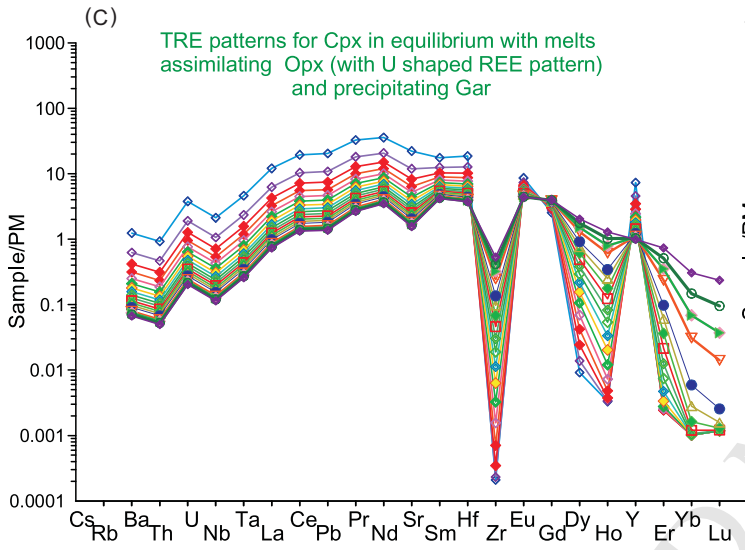
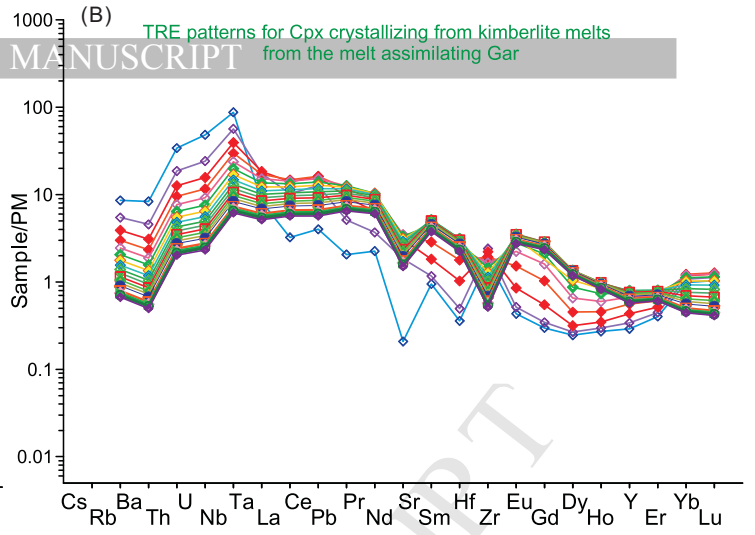
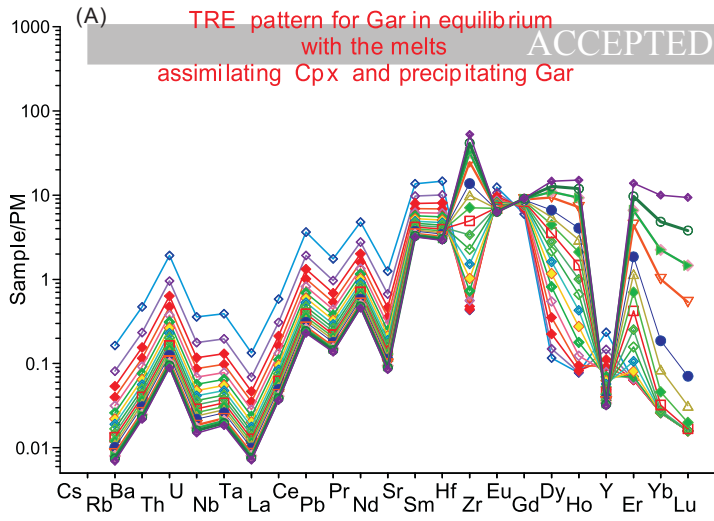


Field for partition coefficients Cpx/Gar for Finsch peridotites (Lazarov et al., 2013)



Partition coefficients Cpx/Ilm





- Mantle column beneath Dalnyaya kimberlite pipe consist of several (5) layers heated from bottom
- Peridotite mantle beneath Dalnyaya interacted with protokimberlite melts in several stages
- Many mineral associations in the mantle column are not thermally and chemically equilibrated
- SCLM beneath Dalnyaya pipe contains only small amounts of eclogites and pyroxenites

ACCEPTED MANUSCRIPT